Synthesis, Diastereomer Separation, Optoelectronic and Structural Properties of Dinuclear Cyclometalated Iridium(III) Complexes with Bridging Diarylhydrazide Ligands

Daniel G. Congrave, Yu-ting Hsu, Andrei S. Batsanov, Andrew Beeby and Martin R. Bryce*

Department of Chemistry, Durham University, South Road, Durham, DH1 3LE, UK

ABSTRACT: A series of diiridium complexes **13–16** bridged by diarylhydrazine ligands and cyclometalated by phenylpyridine or phenylpyrazole ligands was synthesized. In all cases the ΛΔ *meso* and ΛΛ/ΔΔ *rac* diastereomers were separated and characterized by single-crystal X-ray diffraction, revealing intramolecular π–π stacking between arenes of the bridging and cyclometalating ligands. Density functional theory (DFT) calculations show that in general the HOMOs are mainly localized on the iridium centers, the cyclometalating phenyl moieties and the central hydrazide components of the bridging ligands, while the LUMOs are primarily localized on the *N*-heterocycles (pyridine or pyrazole) of the cyclometalating ligands. This series of complexes, especially with the separated diastereomers, provides an ideal opportunity to study the effects of subtle structural changes on the optoelectronic properties of diiridium systems: significant differences are observed between the *rac* and *meso* isomers in some cases. A cyclic voltammetric study of the electrochemical properties of the eight complexes reveals strong intramolecular interactions between the iridium centers. The photophysical properties are reported in solution, and in rigid poly(methyl methacrylate) (PMMA) or 2-methyltetrahydrofuran (2-MeTHF) (at 77 K) matrices where some of the complexes are strongly emissive in the turquoise and green regions (Φ_{PL} 42–68 ±10%) due to matrix-induced restricted intramolecular motion (RIM).

INTRODUCTION

Luminescent Ir(III) complexes have been widely employed in a diverse range of applications,[1] such as photocatalysis,[2] biological labelling[2–4] and sensing.[5] Moreover, they have received particular attention as phosphorescent emitters in organic light-emitting devices (OLEDs) and light-emitting electrochemical cells (LECs),[6,7] where heavy atom induced spin-orbit coupling theoretically enables the harvesting of all electro-generated excitons. Such complexes exhibit a range of favorable properties, such as high quantum efficiency (Φ), rather short phosphorescence lifetimes (τ_p), reversible electrochemistry and synthetic versatility, while being sufficiently robust to often withstand thermal evaporation as a means of device fabrication.[2,8,9] Cyclometalated Ir(III) complexes feature metal-ligand-based luminescent properties and high energy non-emissive metal-centered (MC) states, which enables broad color tuning through structural variation.[8]

Cyclometalated diiridium complexes are frequently encountered in the form of μ-dichloro-bridged dimers, which were first reported in 1974 by Nonoyama[10] and are usually synthesized according to Watts' procedure.[11] Such complexes have found widespread use as precursors to cyclometalated heteroleptic and homoleptic monoiridium complexes.[12,13] However, μ-dichloro-bridged dimers are generally poorly emissive[14,15] (apart from a few recent exceptions[16,17]), a feature common to many diiridium systems, e.g. **1**, **2** and **3** (Figure 1).[18–29] Consequently, for luminescence applications research has primarily concentrated on monoiridium complexes.[30,31]

Nevertheless, the study of phosphorescent diiridium complexes is a rapidly expanding topic and a range of complexes with various conjugated bridging ligands have been reported to possess efficient photo- (PL) and electroluminescence (EL).[32–37] Impressive solution photoluminescence quantum yields (PLQYs) of up to 100% have been reported by Williams, Kozhevnikov and coworkers (compound **4**),[36,38] while solution-processed OLEDs with external quantum efficiencies (EQEs) of >10% have been reported by our group (complex **5**)[39] and also the groups of Zhou and Wong (complex **6**).[40]

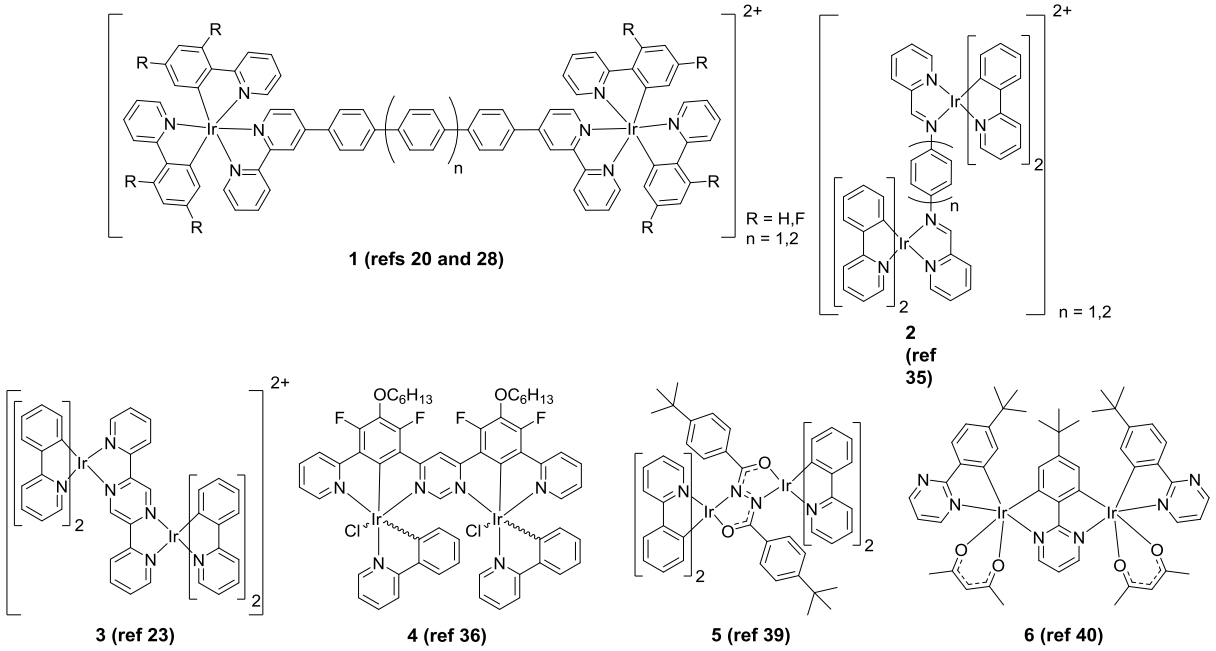

Figure 1. Representative diiridium complexes from the literature.

These examples demonstrate that correctly designed diiridium complexes can overcome the limitation of poor luminescence and present a feasible alternative to typical monoiridium systems.[38]

An important feature of the bridging ligands within diiridium complexes is that they provide an increased potential for structural variation compared to monoiridium systems.[37,41–43] Bimetallic complexes also present a number of other potential advantages, such as increased spin-orbit coupling due to the presence of multiple metal centers (which may lead to an increase in the radiative rate constant (k_r)), easier access to efficient red emitters due to conjugated bridging units,[36,38] higher stability due to the improved chelating effect of a bridging ligand, and the possibility of dual emission.

To obtain high efficiency phosphorescence, it is important to limit non-radiative deactivation (quantified by the non-radiative rate constant (k_{nr})) of the excited complex and this has been achieved through rigidification of the phosphor.[44–46] In diiridium complexes, which incorporate conjugated bridging ligands, theoretical calculations often predict that a degree of frontier orbital character is localized on the bridging unit.[23,26,29,32,35,37–40,42] In these cases a highly flexible bridge is expected to promote non-radiative processes and weaken emission. Consequently, the majority of the reported diiridium complexes that possess high solution state PLQYs incorporate rigid bridging units (such as compounds **4** and **6**).[32,36–37] Highly emissive complexes featuring flexible bridges are rare: for example, compound **2** shows aggregation induced emission (AIE) but is otherwise non-emissive.[35]

The aim of the present work is to explore the potential of diarylhydrazide bridging ligands, which we first introduced in an initial communication on complex **5**.[39] An interesting design feature of these bridges is that they provide a short conjugative pathway between the two Ir centers. We now present a series of new diiridium complexes (**13–16**) featuring different cyclometalated ligands. In all cases the diastereomers have been separated and characterized by their single-crystal X-ray structures. The electrochemical properties of the complexes have been studied in solution, and the photophysical properties are reported in solution, rigid poly(methyl methacrylate) (PMMA) or 2-methyltetrahydrofuran (2-MeTHF) (77 K) matrices, where some of them are strongly emissive. Density functional theory (DFT) calculations provide further insights into the photophysical properties.

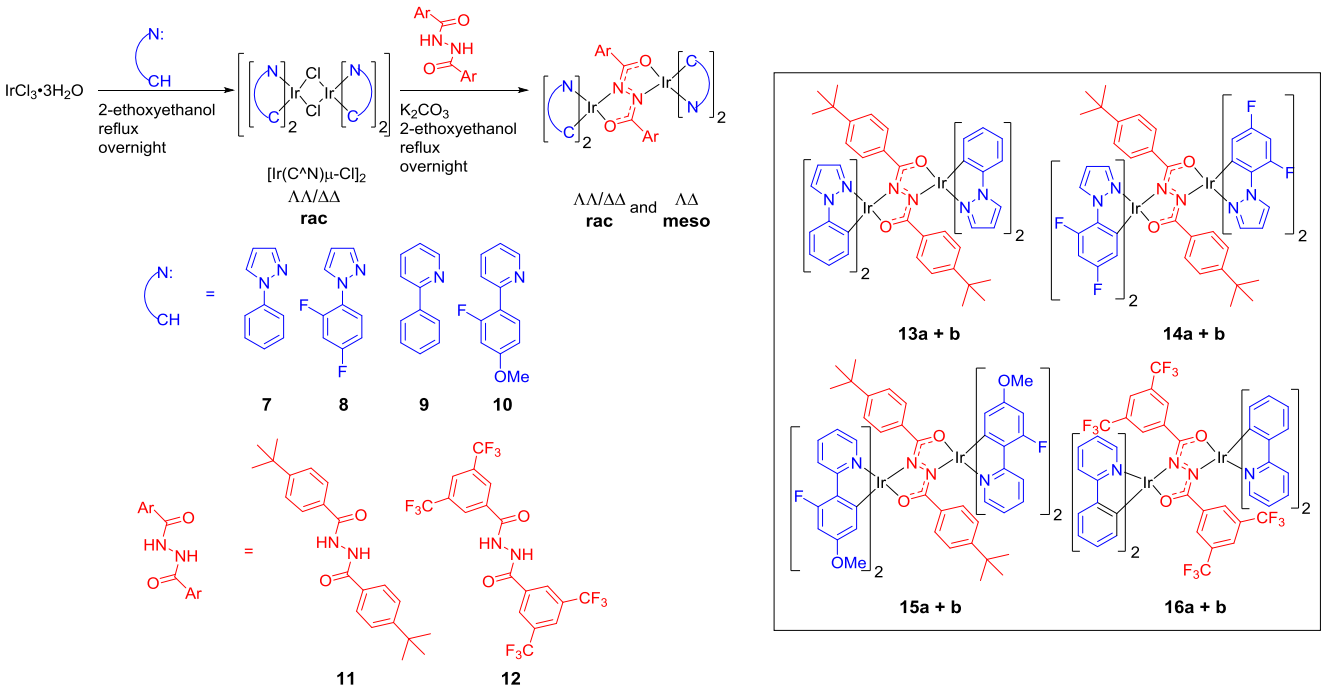

Figure 2. General synthetic scheme and structures of the diiridium complexes **13–16**, **a** = ΛΔ *meso* diastereomers **b** = ΛΛ/ΔΔ *rac* diastereomers, studied in this work.

SYNTHESIS

To synthesize the target diiridium complexes **13–16** the cyclometalating ligands **7–10** were firstly refluxed with $IrCl_3•3H_2O$ in 2-ethoxyethanol to generate the corresponding μ-dichloro-bridged intermediate complexes *in situ* (Figure 2). The intermediate complexes were subsequently cleaved with the hydrazide bridging ligands **11** or **12** in the presence of K_2CO_3 to obtain the diiridium complexes **13–16**. Due to the chiral nature of the iridium centers mixtures of *meso*(ΛΔ, **a**) and *rac* (ΔΔ/ΛΛ, **b**) diastereomers were obtained for all of the complexes, as is commonly observed for cyclometalated diiridium complexes featuring Ir–Ir distances greater than *ca.* 5 Å.[23,26,27,32,34,40,47] (It is noteworthy that with $[Ir(ppy)_2μ–Cl]_2$-type complexes where the Ir–Ir distances are <4 Å only the less sterically congested *rac* ΔΔ/ΛΛ diastereomers have been reported to date[15–18,39,48–55]). For **13–16** the diastereomers were separated by fractional crystallization, silica column chromatography, or a combination of the two techniques. Although stable in methylene chloride (DCM) solution, some of the complexes partially decomposed on silica columns to form small amounts of μ-dichloro-bridged dimers when DCM was used as the eluent. Displacement of non-cyclometalated ligands to form μ-dichloro dimers in the presence of a chloride source in acidic media has been previously reported.[56] This problem was overcome in the present work by the use of K_2CO_3-saturated DCM during purification. The high level of diastereomeric excess of the samples was confirmed by 700 MHz ^1H NMR spectra (as demonstrated for **14a** and **b** in Figure 3 and for the other complexes in Figures S4, S7, S28, S35, S42 and S46). A notable feature is the presence of highly-shielded aromatic protons in the 4.8–5.5 ppm region for all complexes **13–16**. This upfield shift is consistent with intramolecular π–π stacking in the complexes, as observed in the X-ray crystal structures (see below). Additional NMR spectra (where solubility allowed) including $^1H–^1H$ COSY, $^1H–^1H$ NOESY, $^1H–^{13}C$ HSQC and $^1H–^{13}C$ HMBC data are shown in the SI.

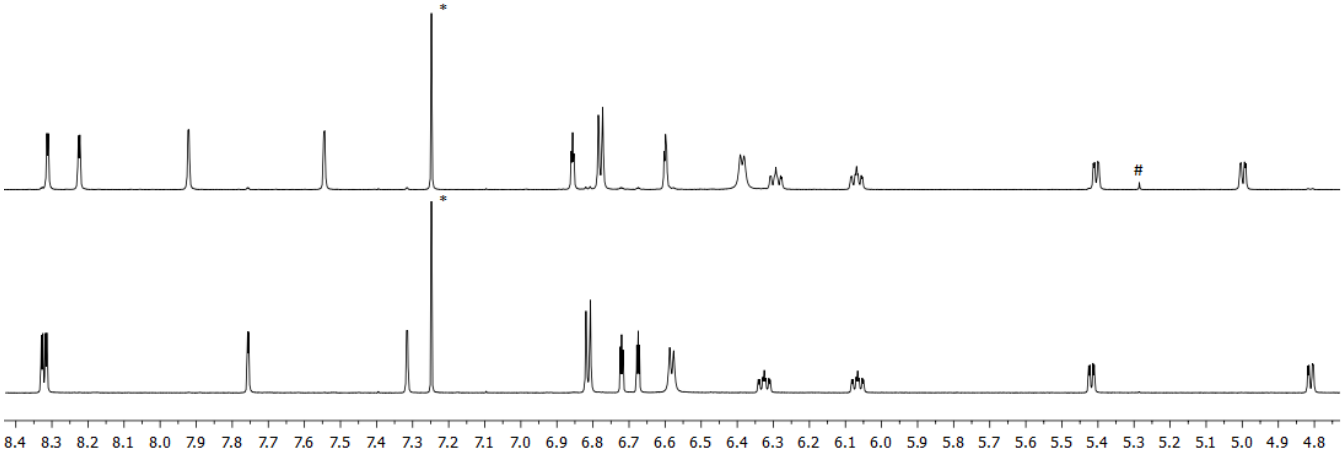

Figure 3. Aromatic regions from the 700 MHz ^1H NMR spectra of **14a** (top) and **14b** (bottom) in $CDCl_3$. * = residual $CHCl_3$ from $CDCl_3$, # = CH_2Cl_2. An inseparable trace amount of **14b** is observed in the spectrum of **14a**.

COMPUTATIONAL STUDY

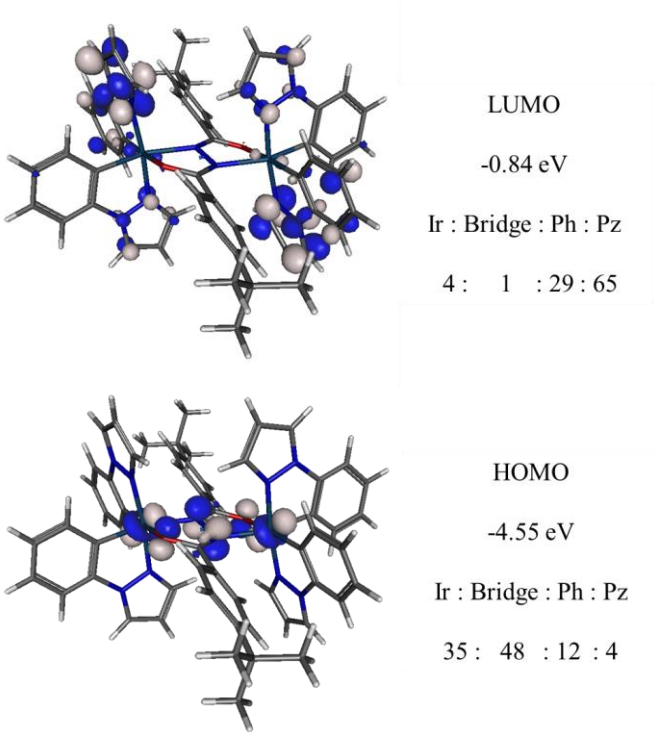

Figure 4. Molecular orbital compositions for complex **13a**.

The optimized ground state S_0 geometries were calculated at the B3LYP/LANL2DZ:3–21G* level with the LANL2DZ pseudopotential for the iridium atoms and the 3–21G* basis set for other atoms. These data are, therefore, directly comparable to previous computational studies on $Ir(ppy)_3$ and other diiridium complexes.[16,39] As a general trend in the optimized geometries, the central bridge CNNC dihedral angle is calculated to be planar (180º) for the *meso* (**a**) isomers, whereas it is twisted for the *rac* (**b**) isomers and displays greater variation between complexes (144–156º). This is ascribed to the greater steric restriction encountered in the *meso* isomers which forces the bridging units to adopt more planar conformations. A similar trend is also observed experimentally in the X-ray crystal structures discussed below.

Molecular orbital calculations were carried out to determine the distribution of the frontier molecular orbitals (FMOs). The FMO compositions of **13a** are shown in Figure 4 as a representative example and the data for all the complexes **13–16** are summarized in Table S3. (FMO plots for all other complexes are shown in Figures S70–S76). In general, except for **13b** where the bridge also features notable LUMO character, the HOMOs are mainly localized on the iridium centers, the cyclometalating phenyl moieties and the central hydrazide components of the bridging ligands, while the LUMOs are primarily localized on the *N*-heterocycles of the cyclometalating ligands. These data are in good agreement with the literature compound **5** (Figure 1).[39] To the best of our knowledge complexes **13** and **14** are the first heteroleptic iridium complexes for which there is significant LUMO localization on the pyrazole groups of the cyclometalating ligands **7** and **8**.[57–59] This is indicative of the high π* energy of the bridge **11**.

The high contribution of the bridge to the HOMO levels of the complexes (non-ancillary character) indicates that the bridging units should play a significant role in the first oxidation potentials of the complexes and also in their excited states. This is in agreement with the electrochemical and photophysical data discussed below.

X-RAY CRYSTALLOGRAPHIC STUDIES

Table 1. Selected geometrical parameters of diiridium complexes (bond distances in Å).

	13a	**13b**	**14a**	**14b** [a]	**14b** [b]	**15a** [c]	**15a** [d]	**15b**	**16a** [e]	**16a** [f]	**16b**
Space group	$P2_1/c$	$P2_1/c$	$P\bar{1}$	$P\bar{1}$	$P2_1/n$	$P\bar{1}$	$P2_1/c$	$Pbcn$	$P\bar{1}$	$P\bar{1}$	C2/c
Mol. symmetry	C_i	--	C_i	--	--	C_i	C_i	C_2	C_i	C_i	C_2
Ir centers	ΛΔ	ΛΛ or ΔΔ	ΛΔ	ΛΛ or ΔΔ	ΛΛ or ΔΔ	ΛΔ	ΛΔ	ΛΛ or ΔΔ	ΛΔ	ΛΔ	ΛΛ or ΔΔ
Ir…Ir	5.013	5.031	4.988	5.007	5.031	5.00	5.029	5.089	5.035, 5.063	5.047	5.095
Ir–C (*trans*-O)	1.992(4)	2.006(6)	2.023(5)	2.000(5)	2.007(4)		1.997(2)	1.996(3)	1.994(3)	1.990(1)	2.000(2)
Ir–C (*trans*-N)	2.004(3)	1.994(6)	2.011(5)	2.003(5)	2.008(4)		1.989(2)	1.998(3)	2.005(3)	1.997(1)	2.006(2)
Ir–N, stacked	2.011(3)	2.005(6)	2.009(5)	2.013(5)	2.015(3)		2.027(2)	2.025(3)	2.027(2)	2.028(1)	2.032(2)
Ir–N, non-stacked	2.018(3)	1.973(6)	2.014(5)	2.018(4)	2.004(3)		2.044(2)	2.032(3)	2.051(2)	2.045(1)	2.044(2)
Bridge geometry											
OCNNCO folding, °	planar	23.9	planar	13.6, 20.8	21.0	planar	planar	29.5	planar	planar	9.8
Ir displacement, Å	0.60	0.18	0.06	0.06, 0.16	0.16	0.59	0.57	0.43	0.46, 0.33	0.46	0.10
Ir–O	2.144(3)	2.116(4)	2.102(4)	2.112(4)	2.111(3)		2.154(1)	2.123(2)	2.143(2)	2.154(1)	2.144(1)
Ir–N	2.152(3)	2.156(5)	2.134(4)	2.144(4)	2.160(3)		2.155(2)	2.181(2)	2.164(2)	2.162(1)	2.174(1)
N–N	1.436(6)	1.439(7)	1.441(8)	1.444(6)	1.447(4)		1.442(3)	1.459(5)	1.444(4)	1.434(2)	1.440(3)
N–C	1.307(5)	1.324(8)	1.308(6)	1.308(6)	1.306(5)		1.315(2)	1.313(4)	1.308(3)	1.316(1)	1.313(2)
C–O	1.295(4)	1.292(8)	1.295(6)	1.286(6)	1.288(4)		1.288(2)	1.285(4)	1.283(3)	1.280(1)	1.281(2)
Intramolecular stacking (π–π)											
Θ, [g]	22.1	12.3, 20.3	12.2	20.6, 27.2, 16.5, 15.3	11.9, 9.4	22	12.0	15.5	7.2, 8.2	6.6	7.6
D, Å [h]	3.52	3.35, 3.57	3.26	3.64, 3.66, 3.47, 3.47	3.39, 3.42	3.54	3.40	3.40	3.43, 3.36	3.39	3.36

[a] **14b**·DCM, average of two independent molecules; [b] **14b**·2DCM·½C_6H_{14}, [c] **15a**·4DCM, major component (bond distances are unreliable due to all-molecule disorder); [d] **15a**·1.84MeOH·0.16DCM; [e] **16a**·½CD_2Cl_2, average of two independent molecules; [f] **16a**·2CD_2Cl_2; [g] inter-planar angle between the cyclometalating ligand and arene ring *A* of the bridging ligand (see **14a**, Figure 5); [h] distance between the cyclometalating ligand plane and the centroid of ring *A*

The molecular structures of complexes **13–16** were studied by single-crystal X-ray crystallography. Important parameters are summarized in Table 1. All structures except **14a** and **16b** (Figure 5) contain solvent of crystallization, which is usually disordered.

In all *meso* (**a**) complexes, the *molecule* is rigorously centrosymmetric, i.e. lies on a crystallographic inversion center (at the midpoint of the N–N bond) which relates the two Ir centers. The *rac* (**b**) (ΛΛ or ΔΔ) isomers either lie on a crystallographic two-fold axis, or have no crystallographic symmetry, but the *crystal* is always centrosymmetric and hence racemic. In each case, both Ir atoms have distorted octahedral coordination, involving one N and one O atom of the bridge, and two C^N cyclometalating ligands arranged with their coordinating N atoms *trans* and axial, as expected.[9,39] Complex **14b** was studied in two different solvates (Figures S53 and S54), one of the structures containing two symmetrically independent molecules, and the same applies to **16a** (Figures S58 and S59). In each case, different crystal packing facilitates relatively minor changes in the molecular conformations and practically no differences in the bond distances.

In all *meso* (**a**) complexes the central bridging hydrazide (OCNNCO) moiety is planar (notably in accurate agreement with the aforementioned geometry optimized DFT structures) with the

two Ir atoms tilting from their planes in opposite directions by 0.3–0.6 Å (except **14a** where they are almost coplanar). In *rac* (**b**) forms, the bridge is folded along the N–N bond (again in good agreement with DFT): the two OCNN planes form an angle of 10 to 30°, whereas the Ir atoms deviate from these planes less than in *meso* (**a**) forms (by 0.1–0.4 Å).

In each complex, either aryl substituent of the bridging ligand is stacked face-to-face (π–π) with a cyclometalating ligand (Figure 5). Ring *A* overlaps mainly with the phenyl ring (*B*) of the latter, although in most structures (especially strongly in **15b**) it is shifted towards the pyridyl or pyrazole ring in a quasi-graphitic fashion, whereas in **13b**, **14a** and **14b**·DCM, ring *A* slips in the opposite direction (Figures S62 and S63). The interplanar angles (Θ) of 6.6–27.2 ° and mean separations (*D*) of 3.26–3.66 Å between the overlapping moieties (Table 1) are common for arene stacking. These are rare examples of intramolecular π–π interactions between bridging and peripheral ligands. Indeed, we are not aware of any previous examples in cyclometalated diiridium systems, although intramolecular π–π interactions have been studied in neutral[60] and cationic monoiridium complexes.[57,61,62]

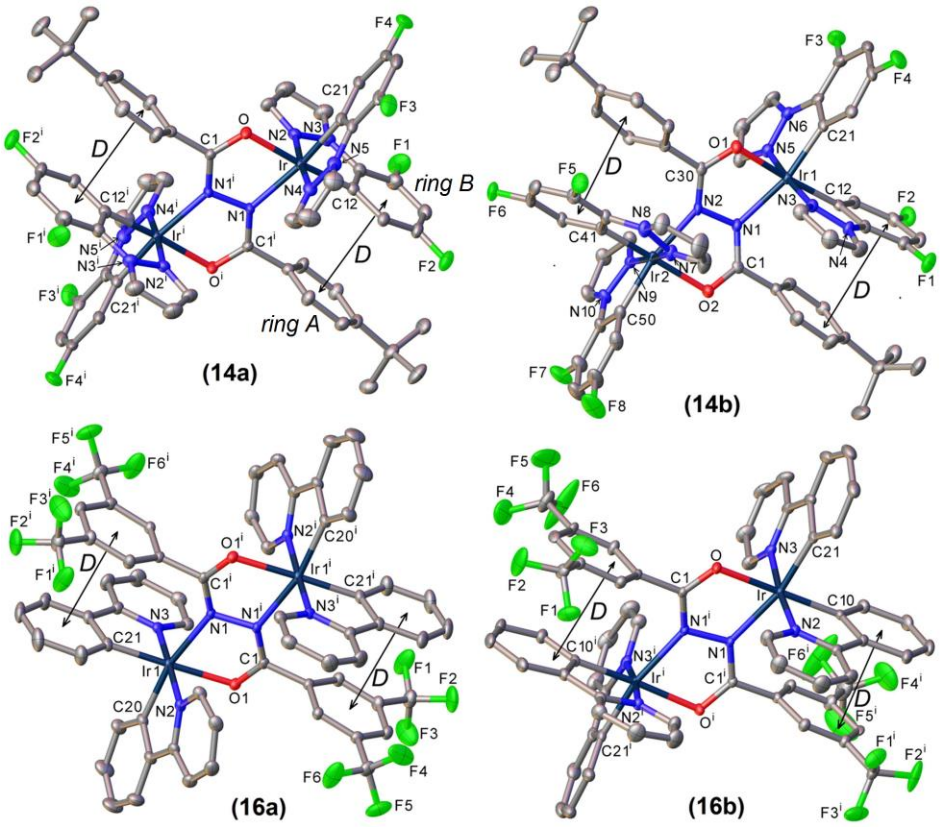

Figure 5. X-ray molecular structures of **14a**, **14b**, **16a** and **16b**. Thermal ellipsoids are drawn at the 50% probability level, H atoms are omitted for clarity. Primed atoms are generated by a crystallographic inversion center (**14a**, **16a**) or a twofold axis (**16b**). Vector *D* identifies intramolecular π–π interactions (see Table 1).

ELECTROCHEMICAL AND PHOTOPHYSICAL STUDIES

The oxidation potentials of the diiridium complexes **13**–**16** were obtained by cyclic voltammetry (CV) (Figure 6) and are listed in Table 2. All complexes display two oxidation waves which are assigned to sequential oxidation of the iridium atoms (Ir^{3+}/ Ir^{4+} redox couples) and also indicate electronic coupling between the two centers through the bridging units. The trend in the first oxidation potentials is **14** > **16** > **15** > **13**. This is in line with the strength of the electron withdrawing substituents on the phenyl rings of the cyclometalating ligands and also correlates with the DFT predictions (above) that the bridge phenyl moieties do not possess HOMO character. This reduces the effect of the strongly withdrawing CF_3 groups on the oxidation potentials of **16a** and **16b**. As a general trend, DFT calculations overestimate the HOMO energies of the diiridium complexes compared to the experimental values (Table 2). Reduction processes were not observed down to *ca.* –2.5 V vs. FcH/FcH^+ (Representative voltammograms for complexes **13b** and **15b** are presented in Figures S67 + S68).

An interesting feature of the CV data is that significantly different oxidation potentials are reproducibly observed for both species **13a** and **13b**, in particular for the first oxidation process ($\Delta E_{1/2}$ for $E^{ox(1)}$ = 60 mV). When a 1:1 mixture was analyzed (Table 2) intermediary oxidation potentials were observed compared to the diastereomerically pure samples, although the oxidation processes for each diastereomer could not be resolved by differential pulse voltammetry (Figure S69). There is also a significant difference in the oxidation potentials between the two diastereomers **14a** and **14b**.

The differences in the electrochemical properties of the diastereomers is ascribed to the different molecular symme-

tries of the complexes (*meso* **a** = C_i, *rac* **b** = C_2) and the fact that diastereomers are known to commonly exhibit differing physical properties. A similar difference between the oxidation potentials of diiridium diastereomers has been previously reported for complex **6**.[40] Large differences in the CNNC dihedral angles of the bridges for the optimized geometries of the diastereomers (see above) could also be related to some of the observed differences in electrochemical properties between isomers.

For the phenylpyridine complexes **15** and **16** the peak splittings ($\Delta E_{1/2}$) (Table 2) between the two oxidation processes are smaller than for the phenylpyrazole analogs **13** and **14**, in line with the calculated lower HOMO contributions from the bridges of **15** and **16** (Table S3). The lowest $\Delta E_{1/2}$ values (*ca.* 250 mV vs. >400 mV for all other complexes) are observed for complexes **16a** and **b**, as expected from the functionalization of the bridge **12** with strongly electron-withdrawing CF_3 groups which results in lower bridge HOMO contributions (Table S3). The electrochemical properties of the diastereomers of the phenylpyridine-functionalized complexes **15** and **16** are very similar.

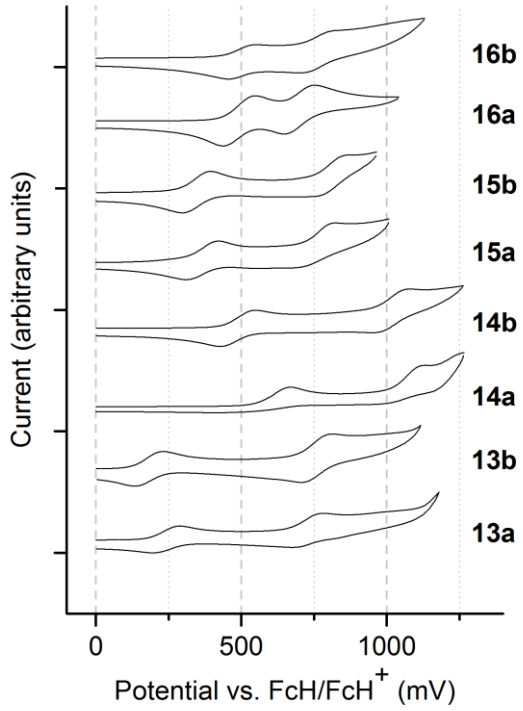

Figure 6. Cyclic voltammograms in 0.1 M *n*-Bu_4NPF_6/ DCM showing the oxidation processes for **13–16**.

Table 2.Oxidation potentials for the Ir^{3+}/ Ir^{4+} couples (E^{ox}, V) of compounds **13–16** referenced to FcH/ FcH^+ = 0.00 V. $E_{1/2}$ values are quoted for electrochemically reversible oxidations.

Complex	Isomer	$E^{ox(1)}$ /V E_{pa}/ E_{pc} [$E_{1/2}$]	$E^{ox(2)}$ /V E_{pa} /E_{pc} [$E_{1/2}$]	$\Delta E_{1/2}$ /V	HOMO /eV[a]	HOMO /eV[b]	LUMO /eV[b]
13	**a** *meso*	0.29/ 0.21 [0.25]	0.78/ 0.69 [0.73]	0.48	–5.05	–4.55	–0.84
	b *rac*	0.23/ 0.15 [0.19]	0.82/ 0.73 [0.77]	0.58	–4.99	–4.52	–0.89
	a + **b** 1:1 *mix*	0.27/ 0.17 [0.22]	0.81/ 0.72 [0.76]	0.54	–5.02	-	-
14	**a** *meso*	0.67/ 0.57	1.11/ 0.96	0.41	–5.42	–5.09	–1.16
	b *rac*	0.55/ 0.44 [0.49]	1.08/ 0.97 [1.03]	0.54	–5.29	–5.05	–1.10
15	**a** *meso*	0.42/ 0.34 [0.38]	0.84/ 0.72	0.40	–5.18	–4.62	–1.26
	b *rac*	0.42/ 0.34 [0.38]	0.88/ 0.76	0.44	–5.18	–4.82	–1.36
16	**a** *meso*	0.57/ 0.46 [0.52]	0.82/ 0.71 [0.77]	0.25	–5.32	–5.01	–1.63
	b *rac*	0.55/ 0.46 [0.51]	0.82/ 0.71 [0.77]	0.26	–5.31	–5.04	–1.62

[a] HOMO levels calculated from CV potentials by HOMO = –4.8 + ($-E_{1/2}^{ox(1)}$), using ferrocene as the standard. [b] Frontier orbital energies calculated from optimized geometries at B3LYP/LANL2DZ:3–21G* level.

The absorption and emission spectra for the diiridium complexes are shown in Figures 7–9 and S64–66 and the key data are listed in Table 3. For the phenylpyrazole complexes **13** and **14**, the bands in the absorption spectra (Figure S64, Table 3) in the 230–270 nm region are ascribed to spin-allowed ligand-centered (LC) $^1\pi$–π* transitions, while the longer wavelength bands which extend to 400 nm are assigned to both singlet and triplet metal-to-ligand charge transfer states (^{1}MLCT and ^{3}MLCT) following literature precedents.[13] Such high energy onsets of absorption (*ca.* 420 and 380 nm) indicate high triplet energies (E_T) of *ca.* 3.0 and 3.3 eV for **13** and **14**, respectively. For the phenylpyridine complexes **15** and **16** similar assignments apply to the absorption spectra (Figure 7, Table 3): $^1\pi$–π* 250–350 nm, ^{1}MLCT and ^{3}MLCT 350–500 nm.[13,63]

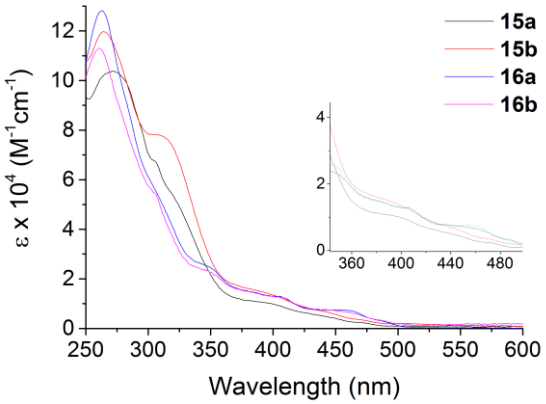

Figure 7. Absorption spectra of complexes **15** and **16** recorded in room temperature DCM solutions. Inset: expansions of the 360–480 nm regions of the spectra.

Photoluminescence could not be detected for the phenylpyrazole complexes **13** and **14** at room temperature in DCM solutions (Table 3). This can be explained by considering thermal population of low-lying non-emissive MC excited states at room temperature.[64] This is promoted by the inadequate crystal field strength of the ligands, which combined with the high E_T values of the complexes leads to d–d* gaps (MC energies) comparable to the MLCT energies. This explanation has been previously suggested for non-emissive homoleptic phenylpyrazole complexes,[65] which like **13** and **14** are predicted to feature significant LUMO contribution from electron rich pyrazole moieties and have large E_T values.

In room temperature DCM solutions, complexes **15** (Figure S65) and **16** are poorly emissive in the turquoise and green regions (Φ_{PL} <1% and nanosecond-scale lifetimes) (Table 3), which is ascribed to facile non-radiative deactivation of their excited states. This is evidenced by their non-radiative rate constants (k_{nr}) (Table 3) which are exceptionally high (e.g. 8.3×10^8 s^{-1} for **16a** and **b**), even in comparison to k_{nr} for $[Ir(ppy)_2\mu\text{-}Cl]_2$ (8.0×10^6 s^{-1})[17] - a diiridium complex commonly known to be poorly emissive (PLQY = 0.5% in toluene, 0.1% in DCM).[14,17]

When doped into poly(methyl methacrylate) (PMMA) (Figure 8), the PLQYs increase by 2–3 orders of magnitude for complexes **15** and **16**, respectively, with observed microsecond-scale lifetimes (Table 3). This is due to the comparable decreases in the values of k_{nr} for the complexes (by 2–3 orders of magnitude) rather than increases in the values of k_r, which are on the order of 10^5 s^{-1} for **15** and **16** in both DCM and PMMA (comparable to $Ir(ppy)_3$ $k_r = 2.1 \times 10^5$ s^{-1}).[13]

As the cyclometalating ligands in **15** and **16** have been previously incorporated into complexes that are highly emissive in solution[13,66] it can be concluded that the bridging ligands play a significant role in the photophysical properties of the complexes in the present study (in agreement with the DFT and electrochemistry data above) and are most likely responsible for their matrix-dependent behavior. In room temperature DCM solutions the highly flexible bridges facilitate non-radiative decay via intramolecular motion which quenches the emission. When the complexes are doped into rigid PMMA matrices, this property is suppressed leading to large increases in PLQY. Moreover, neat films of complexes **15** and **16** drop-cast from DCM solutions were found to be non-emissive (presumably due to triplet–triplet annihilation),[67,68] strengthening our conclusion that this phenomenon occurs in PMMA due to matrix-induced restricted intramolecular motion (RIM), rather than an intermolecular interaction between the diiridium complexes.

Functionalization with electron-withdrawing groups of the cyclometalating or bridging ligands in complexes **15** and **16**, respectively, each lead to hypsochromic shifts in emission wavelength compared to the literature compound **5** (Figure 1) (λ_{max} PL = 521/ 523 nm).[39] These observations indicate that variation of either the bridging or cyclometalating ligands can be used to tune the color of this diiridium system.

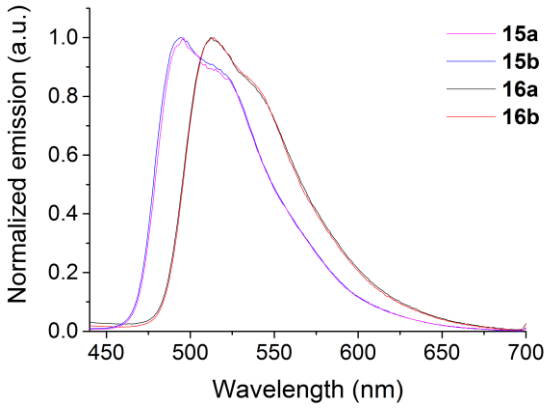

Figure 8. Normalized emission spectra of complexes **15** and **16** doped into PMMA at 1% wt. λ_{exc} = 355 nm.

Emission spectra (Figure S66) recorded in 2-MeTHF at 77 K for complexes **15** and **16** show lifetimes increased to the microsecond-scale due to the expected reduction in vibrations (Table 3). Well-resolved vibronic structures at this temperature may also be indicative of a high LC contribution to their excited states.[69] Within experimental error there is no significant variation in PL properties between the diastereomers for **15** and **16**.

Our explanation regarding the non-emissive properties of complexes **13** and **14** is reinforced by the photophysical data obtained in PMMA at room temperature and in 2-MeTHF at 77 K (Table 3). Doping the complexes into rigid PMMA matrices is insufficient to prevent non-radiative quenching, and, therefore, we propose that the non-emissive properties of the complexes are not solely due to bridge flexibility. However, cooling the complexes down to 77 K alters the Boltzmann distribution and suppresses thermal population of the non-radiative MC states,[13,65] giving rise to emission (Figure 9) with microsecond-scale lifetimes (Table 3). At 77 K, other than weak emission at *ca.* 400–450 nm (which we assign to emission from states of LC/ MLCT character)[13] broad low energy emission bands (450–800 nm) centered at *ca.* 550 and 590 nm are also observed for complexes **13/ 14a** and **13/ 14b**, respectively. This emission is reminiscent of that previously reported at room temperature for a heteroleptic phenylimidazole-functionalized monoiridium complex by Nazeeruddin et al.,[70] where the broad emission was suggested to originate from multiple degenerate emissive states of mixed character. This explana-

tion may also apply to complexes **13** and **14** which are also heteroleptic Ir complexes featuring diazole cyclometalating ligands. The wavelength of the broad bands appears to be dependent on the stereochemistry of the complexes and almost independent of substitution on the phenylpyrazole ligands, indicating that the differing molecular symmetry of diiridium diastereomers can have a significant influence on their photophysical properties. This feature is not generally observed in diiridium complexes[21,40] and may be related to the higher LUMO level of the pyrazole ligands in **13** and **14**.

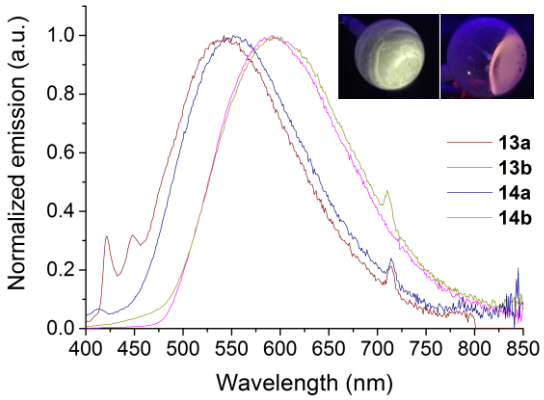

Figure 9. Normalized emission spectra of complexes **13** and **14** in 2-MeTHF glasses at 77 K. λ_{exc} = 355 nm. Inset: photographs of the emission from **13a** (left) and **13b** (right) under irradiation from a 365 nm UV lamp. The peaks at ~710 nm are the second-order diffraction of the scattered excitation beam.

.

Table 3. Summary of the key photoluminescence data for compounds **13–16**.

		Solution[a]						2-MeTHF glass[b]		Doped into PMMA 1% wt.[d]				
Complex	**Isomer**	**λ_{abs} /nm (ε × 10^4 / $M^{-1}cm^{-1}$)**	**$\lambda_{max\ em}$ /nm**	**PLQY /% (± 5%)**	**τ_p /ns**	**k_r /× 10^5 s^{-1}**	**k_{nr} /× 10^5 s^{-1}**	**$\lambda_{max\ em}$ /nm**	**τ_p /µs**	**$\lambda_{max\ em}$ /nm**	**PLQY /% (± 10%)**	**τ_p /µs**	**k_r /× 10^5 s^{-1}**	**k_{nr} /× 10^5 s^{-1}**
13	**a** *meso*	224 (8.79), 280sh (3.41), 305 (2.47), 341 (1.22), 383 (0.36)						(421, 448) 542	8.7					
	b *rac*	234 (8.53), 281sh (3.75), 308 (2.21), 344 (1.20), 383 (0.36)						(424, 443) 591	7.7					
14	**a** *meso*	222 (8.88), 250sh (6.57), 260sh (5.59), 294 (2.49), 326 (1.34), 364 (0.26)	Non-emissive[c]					(394, 414) 552	26.2	Non-emissive[c]				
	b *rac*	226 (8.00), 249sh (6.61), 295 (2.17), 323 (1.28), 365 (0.23)						(395) 593	7.6					
15	**a** *meso*	272 (10.37), 306 (6.75), 321sh (5.20), 399 (1.00), 440 (0.50), 473 (0.23)	489	0.23	34.2	0.58	291.8	479	3.7	493	58	1.5	3.87	2.80
	b *rac*	264 (12.00), 313 (7.73), 393 (1.45), 445 (0.64), 474 (0.33)	493	0.23	51.8	0.39	192.7	481	3.6	494	68	1.6	4.25	2.00
16	**a** *meso*	262 (12.82), 306sh (5.57), 350 (2.50), 383 (1.48), 408 (1.26), 462 (0.72), 489 (0.32)	514	0.03	1.2	2.50	8331	502	3.7	512	45	1.7	2.65	3.24
	b *rac*	260 (11.30), 306 (5.43), 351 (2.25), 383 (1.48), 461 (0.63)	513	0.03	1.2	2.50	8331	499	4.4	515	42	1.7	2.47	3.41

[a]Solution photoluminescence measurements were recorded in degassed DCM solutions at *ca.* 20 ºC with an excitation wavelength of 355 nm with $Ir(ppy)_3$ as standard (Φ = 0.46).[66] Absorption spectra were recorded in aerated acetonitrile for **13** and **14** and aerated DCM for **15** and **16**, sh = shoulder. [b]Measured at 77 K using an excitation wavelength of 355 nm. [c]Non-emissive is defined as PLQY <0.03%. [d]Measured in an integrating sphere under air using an excitation wavelength of 355 nm. $\tau_p = 1/ k_{nr} + k_r$.

CONCLUSIONS

In conclusion, we have synthesized four new diarylhydrazide-bridged diiridium complexes **13–16** for which the diastereomers have been separated and their photophysical, electrochemical and structural properties studied in detail.

Significant differences in photophysical and electrochemical properties between diastereomers were observed for the phenylpyrazole-functionalized complexes **13** and **14**, whereas this is not the case for the phenylpyridine complexes **15** and **16**. The emissive properties of **15** and **16** were found to drastically improve upon doping the complexes into solid PMMA matrices, due to matrix-induced RIM (PLQY increases of 2–3 orders of magnitude compared with their DCM solutions). DFT calculations have provided additional insights into the photophysical properties, and the calculated geometries of the central bridging units are in accurate agreement with single-crystal X-ray diffraction data. We also present rare examples of intramolecular π–π stacking between the bridging and peripheral ligands of a cyclometalated diiridium complex. This interesting feature, combined with the scope for new structural variations in the cyclometalating ligands and the

bridges, should increase the appeal of diiridium complexes as an important platform for fundamental studies and for optoelectronic applications.

EXPERIMENTAL SECTION

General

^{1}H, ^{13}C and ^{19}F NMR spectra were recorded on Bruker Avance 400 MHz, Varian Mercury 200, and 400 MHz, Varian Inova 500 MHz or Varian VNMRS 600 and 700 MHz spectrometers. All spectra were referenced against the residual solvent signal and peak shifts are reported in ppm. For NMR stability experiments the samples were prepared in the specified deuterated solvent and degassed by three freeze pump thaw cycles, before being irradiated at 254 nm with a 6 W UV lamp or refluxed for the specified time. Electrospray ionisation (ESI) mass spectra were recorded on a Waters Ltd. TQD spectrometer. Atmospheric solids analysis probe (ASAP) mass spectra were recorded on a LCT premier XE spectrometer. Matrix-assisted laser desorption time-of-flight (MALDI–TOF) mass spectra were recorded on a Bruker Daltonik Autoflex II spectrometer running in positive ion reflectron mode. MALDI–TOF samples were prepared in CH_2Cl_2 with *trans*-2-[3-(4-*tert*-butylphenyl)-2-methyl-2-propenylidene]malononitrile (DCTB) as the matrix. Elemental analyses were obtained on an Exeter Analytical Inc. CE-440 elemental analyzer. Reactions requiring an inert atmosphere were carried out under argon which was first passed through a phosphorus pentoxide column. Thin layer chromatography (TLC) was carried out on silica gel (Merck, silica gel 60, F_{254}) or alumina (Merck, neutral alumina 60 type E, F_{254}) plates and visualized using UV light (254, 315, 365 nm). Flash chromatography was carried out using either glass columns or a Biotage® Isolera One™ automated flash chromatography machine on 60 micron silica gel purchased from Fluorochem Ltd. or type WN-6 neutral activity grade super I alumina purchased from Sigma Aldrich Co.

Chemicals

All commercial chemicals were of ≥95% purity and were used as received without further purification. $[Ir(ppy)_2\mu\text{–}Cl]_2$,[11] *N*-phenylpyrazole (**7**),[71] *N*-(2,4-difluorophenyl)pyrazole (**8**)[71], 2-(2-fluoro-4-methoxyphenyl)pyridine (**10**)[66] and *N*,*N*'-bis(4-*tert*-butylphenylbenzoyl)hydrazide (**11**)[72] were all synthesized according to literature procedures. All solvents used were of analytical reagent grade or higher. Anhydrous solvents were dried through a HPLC column on an Innovative Technology Inc. solvent purification system.

Calculations

All calculations were carried out with the Gaussian 09 package.[73] All optimized S_0 geometries of the diiridium complexes were carried out using B3LYP[74,75] with the pseudopotential (LANL2DZ)[76–78] for iridium and 3–21G* basis set for all other atoms.[79,80]All S_0 geometries were true minima based on no imaginary frequencies found. Electronic structure calculations were also carried out on the optimized geometries at B3LYP/LANL2DZ:3–21G*. The MO diagrams and orbital contributions were generated with the aid of Gabedit[81] and GaussSum[82] packages, respectively.

X-ray Crystallography

Single crystals of all diiridium complexes **13–16** suitable for X-ray diffraction (XRD) were grown via slow diffusion of either *n*-hexane or methanol into their near-saturated DCM solutions, other than for **16a** where crystals were obtained via slow evaporation of a CD_2Cl_2 solution. Experiments were carried out on a Bruker 3-circle CCD diffractometer D8 Venture with a PHOTON 100 CMOS area detector, using Mo-*K*α radiation (λ=0.71073 Å) from an Incoatec IμS microsource with focusing mirrors. Crystals were cooled to 120 K using a Cryostream 700 (Oxford Cryosystems) open-flow N_2 gas cryostat. Absorption corrections were performed by numerical integration based on measured crystal shape, or (for **13b**) by semi-empirical method based on Laue equivalents and multiple scans.[83] The structures were solved by Patterson (**13b**, **16a**·$2CD_2Cl_2$) or direct methods using SHELXS software,[84] and refined by full-matrix least squares using SHELXL[85] and OLEX2 software.[86]

Crystallization of **14b** from a DCM/hexane solution proceeds in two Ostwald stages: a DCM di-solvate is precipitated initially (Figure S53), which then re-crystallizes into a mixed DCM-hexane solvate (Figure S54). Similarly, crystallization of **15a** from a DCM-methanol solution, yields first a DCM tetrasolvate (Figure S55) and then a methanol di-solvate with a minor substitution of methanol by DCM (Figure S56). In the metastable form, a large part of the host molecule is disordered, including the Ir atoms, and the abnormally high displacement parameters of the rest also suggest disorder. **13b** (Figure S51) crystallized as a non-merohedral twin with the twin law (1 0 0 0 -1 0 -1/3 0 -1), deconvoluted using PLATON TwinRotMatrix program.[87] Structure **14b**·DCM (Figure S53) is triclinic (space group $P\bar{1}$); the lattice can be transformed to an apparently *C*-centred monoclinic (*a*=32.880, *b*=12.873, *c*=27.590 Å, α=89.87, β=102.81, γ=90.14°) but the atomic structure does not fit this symmetry. Independent experiments with three different crystals revealed in each case a pseudo-merohedral twinning with the twin law (1 0 0 -1 -1 0 0 0 -1) corresponding to the (absent) monoclinic twofold axis. The contribution of the second species was refined to 0.454, 0.195 and 0.0558(2), respectively; the latter experiment was used for the final refinement.

Electrochemistry

Cyclic voltammetry experiments were recorded using a BAS CV50W electrochemical analyzer fitted with a three-electrode system consisting of a Pt disk (Ø = 1.8 mm) as the working electrode, a Pt wire as an auxiliary electrode and an Pt wire as a quasireference electrode. Cyclic voltammetry experiments were conducted at a scan rate of 100 mV/s. Experiments were conducted in either dry DCM or dry 1,2-dimethoxyethane solution with *n*-Bu_4NPF_6 (0.1 M) as the supporting electrolyte. Differential pulse voltammetry experiments were recorded using a PalmSens EmStat^2 potentiostat with PSTrace software. Experiments were conducted with step potentials (E step), pulse potentials (E pulse) and pulse times (t Pulse) of 5 mV, 100 mV, and 0.1 s, respectively, at a scan rate of 10 mV/s. The reference electrode was assumed to be stable and was referenced externally to ferrocene.

Photophysics

General The absorption spectra were measured on either a Unicam UV2-100 spectrometor operated with the Unicam Vision software or a Thermo Scientific Evolution 220 spectrometer with the Thermo Scientific Insight software in quartz cuvettes with a path length of 20 mm. The pure solvent was used for the baseline correction. The extinction coefficients were calculated using the Beer-Lambert Law, $A = \varepsilon cl$. The photoluminescence spectra were recorded on a Horiba Jobin Yvon SPEX Fluorolog 3-22 spectrofluorometer in quartz cuvettes with a path length of 10 mm. All Ir complexes were measured in degassed DCM (repeated freeze-pump-thaw cycles using a turbomolecular pump). The quantum yields of all samples were determined by the comparative method relative to $Ir(ppy)_3$ as a standard (Φ = 0.46

in degassed DCM measured in-house vs. quinine sulphate in 0.5 M H_2SO_4 $\Phi = 0.546$[66]) following the literature procedure.[88] The quantum yields of complexes doped into poly(methyl methacrylate) (PMMA) thin films were recorded on a Horiba Jobin Yvon SPEX Fluorolog 3-22 using an integrating sphere and were calculated according to the literature method.[89] Solid state PLQY data were obtained in triplicate from three samples that were prepared in parallel: the calculated standard error values were ≤10%. Lifetime measurements were recorded using an N_2 laser (337 nm, 10 μJ, 10 Hz) as an excitation source in a custom spectrometer which produced a 1 kHz train of pulses of 20 ns duration.. The luminescence was collected at 90° and focused onto the entrance slit of a monochromator (Bethan TM 300V). The emission was detected by a photon counting PMT and the arrival times of photons at the detector determined using a multichannel scaler. The data were transferred to a PC and analyzed using non-linear regression. The decay data were fitted to exponential functions. Low temperature emission spectra and lifetime data were measured in a DN1704 optical cryostat (Oxford Instruments) with a ITC601 temperature controller (Oxford Instruments).

PMMA film preparation 100 μL of a 1 mg mL^{-1} solution of the diiridium complex in DCM was added to 1 mL of a 10 mg mL^{-1} solution of PMMA in *N*,*N*-dimethylformamide (DMF) and the resulting solution was stirred open to air at room temperature (*ca.* 2 h). The solution was then drop-cast using a Gilson precision pipette onto a 15 x 1 mm circular quartz disk (UQG Optics Ltd., UK) in *ca.* 10 x 50 μL portions, allowing the solvent to evaporate at room temperature under air in between each addition (*ca.* 30 min – 1 h). A final 50 μL portion was then drop-cast onto the quartz disk before it was heated to *ca.* 40 ºC overnight on a hot plate under air. Photophysical analysis was then immediately carried out.

Synthesis

***N*,*N*′-Bis(3,5-bis(trifluoromethyl)benzoyl)hydrazide (12).** Based on a literature procedure for analogs,[90] 3,5-bis(trifluoromethyl)benzoyl chloride (5.00 g, 18.1 mmol, 2.13 eq.) was added dropwise under air to a stirred solution of hydrazine monohydrate (425 mg, 8.49 mmol, 1.00 eq.) in ethanol (10 mL), which was cooled in an ice bath to maintain the reaction temperature below 15 °C. A white precipitate formed immediately. Once the addition was half complete, a solution of Na_2CO_3 (954 mg, 9.00 mmol, 1.06 eq.) in water (10 mL) was added dropwise alongside the remaining 3,5-bis(trifluoromethyl)benzoyl chloride. After the addition of the reagents was completed (*ca.* 20 min), the ice bath was removed and stirring was continued at room temperature for a further 30 min. The reaction mixture was poured into water (50 mL), allowed to settle for 1 h and filtered to collect crude **12** as a white powder (4.35 g, 8.50 mmol, 100%), containing *ca.* 10 mol% of residual mono-acylated intermediate (tentatively identified by ^{1}H NMR). Analytically pure **12** was obtained via recrystallization from 5:1 v/v ethanol/*n*-hexane mixture (60 mL) as white needles (3.91 g, 7.63 mmol, 90%). ^{1}H NMR (400 MHz, DMSO-d_6) δ (ppm) = 11.31 (s, 2H), 8.59 (s, 4H), 8.45 (s, 2H); ^{13}C NMR (101 MHz, DMSO-d_6) δ 163.3 ($C_{C=O}$), 134.7, 131.3 (q, ^2J = 33.4 Hz, C_{quart}), 128.8, 126.3, 123.5 (q, ^1J = 273.0 Hz, C_{CF3}); ^{19}F NMR (376 MHz, DMSO-d_6) δ (ppm) = -61.3 (s, 6F); MS (ASAP): *m/z* 513.0 [MH^+]. Calcd. for $C_{18}H_8F_{12}N_2O_2H^+$: 513.0; *Anal.* Calcd. for $C_{18}H_8F_{12}N_2O_2$: C, 42.21; H, 1.57; N, 5.47. Found: C, 42.16; H, 1.57; N, 5.57.

General procedure for the synthesis of dibenzoylhydrazide-bridged diiridium complexes. $IrCl_3 \cdot 3H_2O$ (1.00 eq.) and the cyclometalating ligand (2.20 eq.) were added to 2-ethoxyethanol (5 mL per 200 mg $IrCl_3 \cdot 3H_2O$) and the mixture was heated to reflux under an argon atmosphere for 24 h to form the dichloro-bridged diiridium intermediate *in situ*. The reaction mixture was then cooled to room temperature before addition of the bridging ligand (0.50 eq.) and K_2CO_3 (5.00 eq.). The mixture was then heated at reflux for a further 24 h before being cooled to room temperature and diluted with water (*ca*. 70 mL per 200 mg $IrCl_3 \cdot 3H_2O$) to yield a colored precipitate, which was isolated via filtration and washed with water (2 × 50 mL).

Complexes 13a + b. Following the general procedure, $IrCl_3 \cdot 3H_2O$ (400 mg, 1.13 mmol, 1.00 eq.), *N*-phenylpyrazole (**7**) (360 mg, 2.50 mmol, 2.21 eq.), *N*,*N*′-bis(4-*tert*-butylbenzoyl)hydrazide (**11**) (200 mg, 0.57 mmol, 0.50 eq.) and K_2CO_3 (780 mg, 5.64 mmol, 4.99 eq.) gave a brown precipitate. The isolated solid was triturated with boiling *n*-hexane (500 mL). The hexane insoluble material was passed through a neutral alumina plug (eluent: DCM sat. K_2CO_3) and purified by fractional crystallization via liquid diffusion from saturated DCM solutions layered with *n*-hexane. This yielded the *meso* isomer (**13a**) as pale green crystals (172 mg, 0.12 mmol, 21%). ^{1}H NMR (700 MHz, $CDCl_3$) δ 7.97 (d, J = 2.8 Hz, $2H_{A3}$), 7.94 (d, J = 2.0 Hz, $2H_{A5}$), 7.90 (d, J = 2.9 Hz, $2H_{B3}$), 7.60 (d, J = 2.1 Hz, $2H_{B5}$), 6.94 (d, J = 7.8 Hz, $2H_{B11}$), 6.77 (t, J = 2.5 Hz, $2H_{A4}$), 6.72 (d, J = 7.8 Hz, $2H_{A11}$), 6.63 (t, J = 7.4 Hz, $2H_{B10}$), 6.58 (d, J = 8.1 Hz, $4H_{C3}$), 6.53 (t, J = 2.5 Hz, $2H_{B4}$), 6.45 (t, J = 7.4 Hz, $4H_{A10/B9}$), 6.38 (d, J = 7.9 Hz, $4H_{C2}$), 6.13 (t, J = 7.5 Hz, $2H_{A9}$), 5.98 (dd, J = 7.7, 1.3 Hz, $2H_{B8}$), 5.54 (d, J = 7.4 Hz $2H_{A8}$), 1.10 (s, $18H_{t\text{-}Bu}$); MS (MALDI–TOF): *m/z* 1308.4 [M^+]. Calcd. for $C_{58}H_{54}Ir_2N_{10}O_2^+$: 1308.4; *Anal.* Calcd. for $C_{58}H_{54}Ir_2N_{10}O_2$: C, 53.28; H, 4.16; N, 10.71. Found: C, 53.19; H, 4.15; N, 10.69. The filtrate from the trituration was mixed with celite (*ca.* 2 g) under reduced pressure and subjected to flash chromatography on silica gel (eluent: gradient *n*-hexane/ DCM sat. K_2CO_3 1:0–1:9 v/v) to yield the crude *rac* isomer (**13b**), which eluted before residual traces of the *meso* isomer. Trituration with hot methanol followed by filtration gave **13b** as a pale green powder (90 mg, 0.07 mmol, 12%). ^{1}H NMR (700 MHz, $CDCl_3$) δ (ppm) = 8.02 (dd, J = 2.9, 0.7 Hz, $2H_{C3}$), 8.01 (dd, J = 3.0, 0.7 Hz, $2H_{A3}$), 7.75 (dd, J = 2.1, 0.7 Hz, $2H_{A5}$), 7.37 (dd, J = 2.1, 0.7 Hz, $2H_{C5}$), 7.03 (dd, J = 7.9, 1.1 Hz, $2H_{B3}$), 6.85 (dd, J = 7.8, 1.2 Hz, $2H_{D3}$), 6.69 (ddd, J = 7.9, 7.2, 1.3 Hz, $2H_{B4}$), 6.65–6.57 (m, $12H_{A4,\ C4,\ E2,\ E3}$), 6.49–6.45 (m, $4H_{D4,\ B5}$), 6.03 (td, J = 7.4, 1.2 Hz, $2H_{D5}$), 5.98 (dd, J = 7.6, 1.3 Hz, $2H_{B6}$), 5.32 (dd, J = 7.6, 1.3 Hz, $2H_{D6}$), 1.10 (s, $18H_{t\text{-}Bu}$); ^{13}C NMR (176 MHz, $CDCl_3$) δ (ppm) = 176.1 ($C_{C=O}$), 149.4 (C_{E1}), 143.5 (C_{B1}), 142.4 (C_{D1}), 137.7 (C_{A5}), 136.6 (C_{C5}), 134.4 (C_{B6}), 133.6 (C_{D6}), 133.4 (C_{E4}), 133.3 (C_{B2}), 133.0 (C_{B2}), 126.6 (C_{A3}), 125.5 (C_{E2}), 125.2 (C_{D5}), 124.6 (C_{C3}), 123.9 (C_{E3}), 121.2 (C_{B4}), 119.4 (C_{D4}), 110.3 (C_{B3}), 109.6 (C_{D3}), 106.6 (C_{A4}), 106.3 (C_{C4}), 34.2 ($C_{t\text{-Bu quart}}$), 31.2 ($C_{t\text{-Bu Me}}$); MS (MALDI–TOF): *m/z* 1308.4 [M^+]. Calcd. for $C_{58}H_{54}Ir_2N_{10}O_2^+$: 1308.4; Anal. Calcd. for $C_{58}H_{54}Ir_2N_{10}O_2$: C, 53.28; H, 4.16; N, 10.71. Found: C, 53.56; H, 4.36; N, 10.49.
Solutions sufficiently concentrated for full assignment of carbon environments and C^N ligand orientation with respect to the bridge could not be obtained for **13a** due to its low solubility in organic solvents.

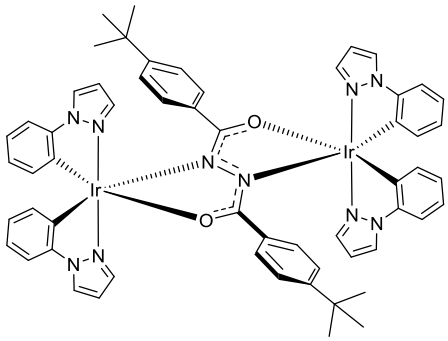

13a

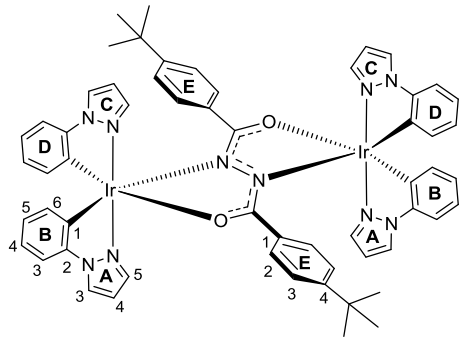

13b

Complexes 14a + b. Following the general procedure, $IrCl_3 \cdot 3H_2O$ (340 mg, 0.96 mmol, 1.00 eq.), *N*-(2,4-difluorophenyl)pyrazole (**8**) (380 mg, 2.11 mmol, 2.20 eq.), *N*,*N*′-bis(4-*tert*-butylbenzoyl)hydrazide (**11**) (170 mg, 0.48 mmol, 0.50 eq.) and K_2CO_3 (665 mg, 4.81 mmol, 5.01 eq.) gave an off-white precipitate. The isolated solid was triturated with boiling *n*-hexane (300 mL). The hexane insoluble material was passed through a neutral alumina plug (eluent: DCM sat. K_2CO_3) and purified by fractional crystallization via liquid diffusion from saturated DCM solutions layered with *n*-hexane. This yielded the *meso* isomer (**14a**) as white crystals (130 mg, 0.09 mmol, 19%). ^{1}H NMR (700 MHz, $CDCl_3$) δ (ppm) = 8.31 (d, *J* = 2.9 Hz, $2H_{A3}$), 8.22 (d, *J* = 3.0 Hz, $2H_{C3}$), 7.92 (d, *J* = 2.1 Hz, $2H_{A5}$), 7.54 (d, *J* = 2.2 Hz, $2H_{C5}$), 6.86 (dd, *J* = 3.0, 2.2 Hz, $2H_{A4}$), 6.78 (d, *J* = 8.7 Hz, $4H_{E3}$), 6.60 (dd, *J* = 3.0, 2.2 Hz, $2H_{C4}$), 6.39 (d, *J* = 7.7 Hz, $4H_{E2}$), 6.29 (ddd, *J* = 11.5, 8.6, 2.5 Hz, $2H_{D4}$), 6.07 (ddd, *J* = 11.4, 8.6, 2.5 Hz, $2H_{B4}$), 5.40 (dd, *J* = 8.5, 2.5 Hz, $2H_{D6}$), 5.00 (dd, *J* = 8.7, 2.5 Hz, $2H_{B6}$), 1.14 (s, $18H_{t\text{-}Bu}$); ^{13}C NMR (176 MHz, $CDCl_3$) δ (ppm) = 176.7 ($C_{C=O}$), 159.6 (dd, *J* = 250.00, 10.51 Hz, C_{D5}), 159.0 (dd, *J* = 248.64, 11.28 Hz, C_{B5}) 150.2 (C_{E1}), 148.6 (dd, *J* = 253.03, 12.73 Hz, C_{D3}), 148.0 (dd, *J* = 251.38, 13.68 Hz, C_{B3}), 136.9 (C_{C5}), 136.2 (C_{A5}), 132.4 (C_{E4}), 130.6 (d, *J* = 15.0 Hz, C_{C3}), 130.2 (d, *J* = 14.6 Hz, C_{A3}), 127.5 (C_{D2}), 126.5 (C_{B2}), 126.03 (C_{E2}), 124.00 (C_{E3}), 115.8 (d, *J* = 18.8 Hz, C_{D1}), 115.2 (d, *J* = 18.7 Hz, C_{B1}), 107.4 (d, *J* = 2.5 Hz, C_{A4}), 107.3 (d, *J* = 2.5 Hz, C_{C4}), 97.8 (dd, *J* = 28.2, 23.4 Hz, C_{D4}), 96.4 (dd, *J* = 28.1, 23.0 Hz, C_{B4}), 34.3 ($C_{t\text{-}Bu\ quart}$), 31.0 ($C_{t\text{-}Bu\ Me}$); ^{19}F NMR (376 MHz, $CDCl_3$) δ -114.5 – -114.4 (m, 4F), -125.8 (dd, *J* = 12.0, 5.5 Hz, 2F), -126.01 (dd, *J* = 11.9, 5.3 Hz, 2F); MS (MALDI–TOF): *m/z* 1452.3 [M^+]. Calcd. for $C_{58}H_{46}F_8Ir_2N_{10}O_2^+$: 1452.3; *Anal.* Calcd. for $C_{58}H_{46}F_8Ir_2N_{10}O_2$: C, 47.99; H, 3.19; N, 9.65. Found: C, 47.92; H, 3.20; N, 9.62. The filtrate from the trituration was mixed with celite (*ca.* 2 g) under reduced pressure and subjected to flash chromatography on silica gel (eluent: gradient *n*-hexane/DCM sat. K_2CO_3 1:0–2:3 v/v) to yield the crude *rac* isomer (**14b**), which eluted before residual traces of the *meso* isomer. Trituration with hot methanol followed by filtration gave **14b** as a white powder (105 mg, 0.07 mmol, 15%) ^{1}H NMR (700 MHz, $CDCl_3$) δ (ppm) = 8.33 (d, *J* = 3.0 Hz ,$2H_{A3}$), 8.32 (d, *J* = 2.9 Hz, $2H_{C3}$), 7.76 (dd, *J* = 2.1, 0.7 Hz, $2H_{A5}$), 7.32 (dd, *J* = 2.1, 0.6 Hz, $2H_{C5}$), 6.81 (d, *J* = 8.4 Hz, $4H_{E3}$), 6.72 (dd, *J* = 3.0, 2.2 Hz, $2H_{A4}$), 6.67 (dd, *J* = 2.9, 2.2 Hz, $2H_{C4}$), 6.58 (d, *J* = 7.8 Hz, $4H_{E2}$), 6.33 (ddd, *J* = 11.5, 8.6, 2.5 Hz, $2H_{B4}$), 6.07 (ddd, *J* = 11.4, 8.6, 2.5 Hz, $2H_{D4}$), 5.42 (dd, *J* = 8.4, 2.5 Hz, $2H_{B6}$), 4.81 (dd, *J* = 8.8, 2.4 Hz, $2H_{D6}$), 1.14 (s, $18H_{t\text{-}Bu}$); ^{13}C NMR (176 MHz, $CDCl_3$) δ (ppm) = 176.4 ($C_{C=O}$), 159.6 (dd, *J* = 250.83, 11.15 Hz, C_{B5}), 158.8 (dd, *J* = 247.73, 12.08 Hz, C_{D5}), 150.7 (C_{E1}), 148.6 (dd, *J* = 251.19, 11.51 Hz, C_{B3}), 148.0 (dd, *J* = 251.19, 13.10 Hz, C_{D3}), 137.3 (C_{A5}), 136.3 (C_{C5}), 132.5 (C_{E4}), 130.7 (d, *J* = 14.9 Hz, C_{A3}), 129.9 (d, *J* = 14.9 Hz, C_{C3}), 127.5 (C_{B1}), 126.6 (C_{D1}), 126.5 (C_{E2}), 124.1 (C_{E3}), 116.0 (d, *J* = 19.5 Hz, C_{B2}), 115.1 (d, *J* = 20.3 Hz, C_{D2}), 107.6 (d, *J* = 2.5 Hz, C_{A4}), 107.1 (d, *J* = 2.5 Hz, C_{C4}), 97.8 (dd, *J* = 27.9, 23.4 Hz, C_{B4}), 96.3 (dd, *J* = 28.2, 23.3 Hz, C_{D4}), 34.3 ($C_{t\text{-}Bu\ quart}$), 31.0 ($C_{t\text{-}Bu\ Me}$); ^{19}F NMR (376 MHz, $CDCl_3$) δ (ppm) = -114.3 – -114.2 (m, 4F), -125.8 (dd, *J* = 12.0, 5.5 Hz, 2F), -126.8 (dd, *J* = 12.0, 5.2 Hz, 2F); MS (MALDI–TOF): *m/z* 1452.3 [M^+]. Calcd. for $C_{58}H_{46}F_8Ir_2N_{10}O_2^+$: 1452.3; *Anal.* Calcd. for $C_{58}H_{46}F_8Ir_2N_{10}O_2$: C, 47.99; H, 3.19; N, 9.65, Calcd. for $C_{58}H_{46}F_8Ir_2N_{10}O_2 \cdot 0.1C_6H_{14}$ (C_6H_{14} is observed in ^{1}H NMR, Figure S21): C, 48.20; H, 3.27; N, 9.59. Found: C, 48.44; H, 3.35; N, 9.46.

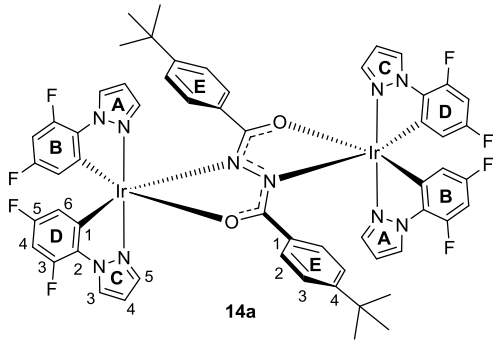

14a

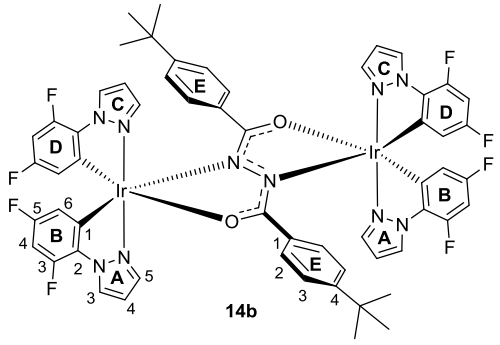

14b

Complexes 15a + b. Following the general procedure, $IrCl_3 \cdot 3H_2O$ (200 mg, 0.57 mmol, 1.00 eq.), 2-(2-fluoro-4-methoxyphenyl)pyridine (**10**) (255 mg, 1.25 mmol, 2.19 eq.), *N*,*N*'-bis(4-*tert*-butylbenzoyl)hydrazide (**11**) (100 mg, 0.28 mmol, 0.50 eq.) and K_2CO_3 (390 mg, 2.82 mmol, 4.95 eq.) gave a yellow precipitate. The isolated solid was extracted into DCM sat. K_2CO_3 (*ca.* 100 mL) and suspended onto celite (*ca.* 2 g) under reduced pressure. The residue was purified via flash chromatography on silica gel (eluent: gradient *n*-hexane/ DCM sat. K_2CO_3 1:0–3:7 v/v). First to elute was the *rac* isomer (**15b**), followed by the *meso* isomer (**15a**). Final purification by trituration with hot methanol gave the diastereomers as yellow powders:

rac (**15b**) (58 mg, 0.04 mmol, 13%). ^{1}H NMR (700 MHz, $CDCl_3$) δ (ppm) = 9.17 (dd, *J* = 5.2, 1.3 Hz, $2H_{A6}$), 8.24 (d, *J* = 5.4 Hz, $2H_{C6}$), 8.13 (d, *J* = 8.5 Hz, $2H_{A3}$), 7.98 (d, *J* = 8.4 Hz, $2H_{C3}$), 7.77 (td, *J* = 7.9, 1.6 Hz, $2H_{A4}$), 7.74 – 7.71 (m, $2H_{C4}$), 7.21 (ddd, *J* = 7.2, 5.5, 1.4 Hz, $2H_{A5}$), 6.93 (ddd, *J* = 7.2, 5.5, 1.4 Hz, $2H_{C5}$), 6.67 (d, *J* = 8.4 Hz, $4H_{E3}$), 6.47 (d, *J* = 8.4 Hz, $4H_{E2}$), 5.98 (dd, *J* = 14.3, 2.3 Hz, $2H_{B4}$), 5.78 (dd, *J* = 14.0, 2.3 Hz, $2H_{D4}$), 5.21 (d, *J* = 2.3 Hz, $2H_{B6}$), 5.05 (d, *J* = 2.3 Hz, $2H_{D6}$), 3.38 (s, $6H_{MeO-B}$), 3.36 (s, $6H_{MeO-D}$), 1.12 (s, $18H_{t\text{-}Bu\ Me}$); ^{13}C NMR (176 MHz, $CDCl_3$) δ (ppm) = 176.2 ($C_{C=O}$), 166.9 (d, *J* = 6.85 Hz, C_{A2}), 166.4 (d, *J* = 5.68 Hz, C_{C2}), 161.6 (d, *J* = 255.91 Hz, C_{B3}), 161.2 (d, *J* = 256.71 Hz, C_{D3}), 160.8 (d, *J* = 11.28 Hz, C_{D5}), 160.1 (d, *J* = 11.82 Hz, C_{B5}), 149.7 (C_{E1}), 148.9 (C_{A6}), 147.5 (C_{C6}), 137.2 (C_{A4}), 136.4 (C_{C4}), 132.4 (C_{E4}), 126.6 (C_{E2}), 124.5 (d, *J* = 4.85 Hz, C_{B1}), 123.6 (C_{E3}), 123.5 (d, *J* = 4.85 Hz, C_{D1}), 122.5 (d, *J* = 17.65 Hz, C_{A3}), 121.4 (d, *J* = 18.69 Hz, C_{C3}), 120.0 (C_{A5}), 119.5 (C_{C5}), 112.9 (C_{B6}), 111.6 (C_{D6}), 95.0 (d, *J* = 27.69 Hz, C_{B4}), 94.1 (d, *J* = 26.31 Hz, C_{D4}), 54.7 (C_{OMe-D}), 54.4 (C_{OMe-B}), 34.2 ($C_{t\text{-}Bu\ quart}$), 31.0 ($C_{t\text{-}Bu\ Me}$); ^{19}F NMR (376 MHz, $CDCl_3$) δ (ppm) = -112.7 (d, *J* = 14.5 Hz, 2F), -113.1 (d, *J* = 14.2 Hz, 2F); MS (MALDI–TOF): *m/z* 1544.4 [M^+]. Calcd. for $C_{70}H_{62}F_4Ir_2N_6O_6^+$: 1544.4; *Anal.* Calcd. for $C_{70}H_{62}F_4Ir_2N_6O_6$: C, 54.46; H, 4.05; N, 5.44. Found: C, 54.35; H, 4.22; N, 5.12.

meso (**15a**) (90 mg, 0.06 mmol, 20%). ^{1}H NMR (700 MHz, $CDCl_3$) δ (ppm) = 9.00 (d, *J* = 5.3 Hz, $2H_{A6/C6}$), 8.75 (d, *J* = 5.3 Hz, $2H_{A6/C6}$), 8.10 – 8.06 (m, $4H_{A3/C3}$), 7.84 (t, *J* = 7.6 Hz, $2H_{A4/C4}$), 7.67 (t, *J* = 7.9 Hz, $2H_{A4/C4}$), 7.30 (t, *J* = 6.7 Hz, $2H_{A5/C5}$), 6.88 (t, *J* = 6.7 Hz, $2H_{A5/C5}$), 6.70 (d, *J* = 7.9 Hz, $4H_{E3}$), 6.35 (d, *J* = 7.8 Hz, $4H_{E2}$), 6.01 (dd, *J* = 14.5, 2.3 Hz, $2H_{B4}$), 5.81 (dd, *J* = 14.2, 2.3 Hz, $2H_{D4}$), 5.29 (d, *J* = 2.3 Hz, $2H_{B6}$), 5.08 (d, *J* = 2.3 Hz, $2H_{D6}$), 3.42 (s, $6H_{MeO\ B}$), 3.38 (s, $6H_{MeO\ D}$), 1.16 (s, $18H_{t\text{-}Bu}$); ^{19}F NMR (376 MHz, CD_2Cl_2) δ (ppm) = -112.8 (d, *J* = 16.9 Hz, 2F), -113.3 (d, *J* = 16.5 Hz, 2f); MS (MALDI–TOF): *m/z* 1544.4 [M^+]. Calcd. for $C_{70}H_{62}F_4Ir_2N_6O_6^+$: 1544.4; *Anal.* Calcd. for $C_{70}H_{62}F_4Ir_2N_6O_6$: C, 54.46; H, 4.05; N, 5.44. Found: C, 54.56; H, 4.15; N, 5.33.
Solutions sufficiently concentrated for full assignment of carbon environments and ligand pyridine–phenyl connectivity could not be obtained for **15a** due to its low solubility in organic solvents.

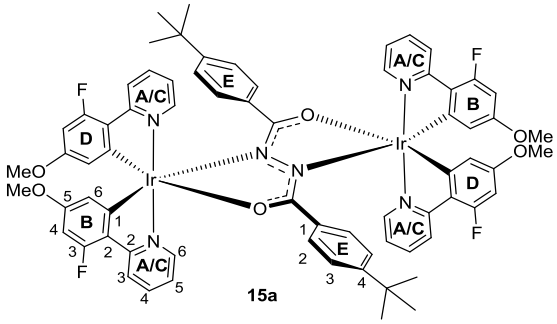

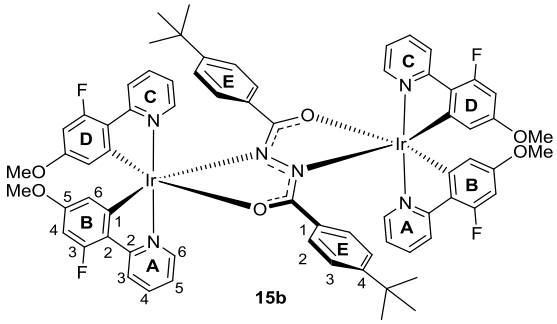

Complexes 16a + b. Following a modification of the general procedure starting directly from the dichloro-bridged intermediate [Ir(ppy)$_2$μ–Cl]$_2$ (400 mg, 0.37 mmol, 1.00 eq.) *N*,*N*′-bis(3,5-bis(trifluoromethyl)benzoyl)hydrazide (**12**) (191 mg, 0.37 mmol, 1.00 eq.) and K_2CO_3 (258 mg, 1.87 mmol, 5.00 eq.) a yellow precipitate was obtained. The isolated solid was then extracted into DCM sat. K_2CO_3 (*ca.* 100 mL) and mixed with celite (*ca.* 2 g) under reduced pressure. The residue was purified via flash chromatography on silica gel (eluent: *n*-hexane/ DCM sat. K_2CO_3 1:1) and both diastereomers were collected as a single fraction. After evaporation of the solvent under reduced pressure, the yellow residue was refluxed in toluene (*ca.* 600 mL) for 10 min before being filtered hot through a glass sinter. The filtrate was then reduced in volume by *ca.* 50 mL and filtered again while hot. This process of reducing the volume by 50 mL followed by hot filtration was repeated a further two times before all of the isolated solids were combined and washed with pentane to afford the *meso* isomer (**16a**) (78 mg, 0.05 mmol, 14%) as a yellow powder. ^{1}H NMR (700 MHz, CD_2Cl_2) δ (ppm) = 9.01 (dd, *J* = 5.5, 1.3 Hz, $2H_{A6}$), 8.76 (dd, *J* = 5.6 Hz, $2H_{B6}$), 7.98 – 7.94 (m, $2H_{A4}$), 7.84 – 7.78 (m, $6H_{A3,B3,B4}$), 7.53 (ddd, *J* = 7.2, 5.5, 1.4 Hz, $2H_{A5}$), 7.47 (bs, $2H_{C2\ or\ 6}$), 7.43 (dd, *J* = 7.7, 1.3 Hz, $2H_{B9}$), 7.27 (s, $2H_{C4}$), 7.16 – 7.09 (m, $4H_{A9,B5}$), 6.75 (t, *J* = 7.0 Hz, $2H_{B10}$), 6.59 (ddd, *J* = 8.2, 7.0, 1.3 Hz, $2H_{B11}$), 6.48 (td, *J* = 7.4, 1.2 Hz, $2H_{A10}$), 6.30 (t, *J* = 7.3 Hz, $2H_{A11}$), 6.01 (bs, $2H_{C2\ or\ 6}$), 5.92 (dd, *J* = 8.2, 1.2 Hz, $2H_{B12}$), 5.85 (dd, *J* = 7.7, 1.1 Hz, $2H_{A12}$); ^{19}F NMR (376 MHz, CD_2Cl_2) δ (ppm) = -63.07 (bs, 6F), -63.18 (bs, 6F); MS (MALDI–TOF): *m/z* 1512.2 [M^+]. Calcd. for $C_{62}H_{38}F_{12}Ir_2N_6O_2^+$: 1512.2; *Anal.* Calcd. for $C_{62}H_{38}F_{12}Ir_2N_6O_2$: C, 49.27; H, 2.53; N, 5.56. Found: C, 49.04; H, 2.55; N, 5.47.
The filtrate from the hot filtrations was mixed with celite (*ca.* 2 g) under reduced pressure before being subjected to flash chromatography on silica gel (eluent: gradient *n*-hexane/ DCM sat. K_2CO_3 1:0–1:1 v/v) to yield the crude *rac* isomer (**16b**), which eluted before residual *meso* isomer. The residue was triturated with boiling methanol (*ca.* 5 mL) and the resulting suspension was cooled in a fridge before being filtered and washed with pentane to afford **16b** as a yellow powder (56 mg, 0.04 mmol, 10%). ^{1}H NMR (700 MHz, CD_2Cl_2) δ (ppm) = 9.24 (dd, *J* = 5.5, 1.4 Hz, $2H_{A6}$), 8.28 (d, 5.2 Hz, $2H_{B6}$), 7.96 – 7.91 (m, $4H_{A4,B4}$), 7.89 (d, *J* = 8.3 Hz, $2H_{A3}$), 7.75 (d, *J* = 8.1 Hz, $2H_{B3}$), 7.50 (ddd, *J* = 7.3, 5.6, 1.5 Hz, $2H_{A5}$), 7.47 (d, *J* = 7.7 Hz, $2H_{A9}$), 7.28 – 7.25 (m, $4H_{B5,C4}$), 7.09 (dd, *J* = 7.6, 1.3 Hz, $2H_{B9}$), 7.08 (bs, $2H_{C2\ or\ 6}$), 6.81 (bs, $2H_{C2\ or\ 6}$), 6.76 (t, *J* = 7.5 Hz, $2H_{A10}$), 6.58 (t, *J* = 8.3 Hz, $2H_{A11}$), 6.50 (t, *J* = 7.4 Hz, $2H_{B10}$), 6.36 (t, *J* = 7.4 Hz, $2H_{B11}$), 5.90 (dd, *J* = 7.7, 1.2 Hz, $2H_{A12}$), 5.85 (dd, *J* = 7.7, 1.1 Hz, $2H_{B12}$); ^{19}F NMR (376 MHz, CD_2Cl_2) δ (ppm) = -62.8 (bs, 6F), -63.2 (bs, 6F); MS (MALDI–TOF): *m/z* 1512.2 [M^+]. Calcd. for $C_{62}H_{38}F_{12}Ir_2N_6O_2^+$: 1512.2; *Anal.* Calcd. for $C_{62}H_{38}F_{12}Ir_2N_6O_2$: C, 49.27; H, 2.53; N, 5.56. Found: C, 48.94; H, 2.65; N, 5.43. Solutions sufficiently concentrated for full assignment of carbon environments could not be obtained for either complex due to low solubility in organic solvents.

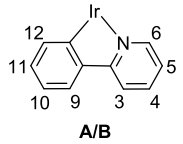

A/B

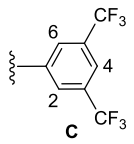

C

ASSOCIATED CONTENT

Supporting Information. NMR spectra of compounds **12**–**16**; Cartesian coordinates of optimized geometries; additional computational, photophysical and electrochemical data and X-ray crystallographic data, including files in CIF format with CCDC numbers 1510118-1510127 and 1511210.

AUTHOR INFORMATION

Corresponding Author

*m.r.bryce@durham.ac.uk

Notes

The authors declare no competing financial interests.

ACKNOWLEDGEMENT

We thank Dr M. A. Fox for helpful discussions of DFT data. We thank EPSRC grant EP/L02621X/1 for funding.

REFERENCES

(1) Chen, Z. Q.; Bian, Z. Q.; Huang, C. H. *Adv. Mater.* **2010**, *22*, 1534–1539.

(2) Lowry, M. S.; Bernhard, S. *Chem. Eur. J.* **2006**, *12*, 7970–7977.

(3) Lo, K. K.-W.; Tsang, K. H.-K.; Sze, K.-S.; Chung, C.-K.; Lee, T. K.-M.; Zhang, K. Y.; Hui, W.-K.; Li, C.-K.; Lau, J. S.-Y.; Ng, D. C.-M.; Zhu, N. *Coord. Chem. Rev.* **2007**, *251*, 2292–2310.

(4) Lo, K. K.-W.; Chung, C.-K.; Ng, D. C.-M.; Zhu, N. *New J. Chem.* **2002**, *26*, 81–88.

(5) Gao, R.; Ho, D. G.; Hernandez, B.; Selke, M.; Murphy, D.; Djurovich, P. I.; Thompson, M. E. *J. Am. Chem. Soc.* **2002**, *124*, 14828–14829.

(6) Choy, W. C. H.; Chan, W. K.; Yuan, Y. *Adv. Mater.* **2014**, *26*, 5368–5398.

(7) Costa, R. D.; Ortí, E.; Bolink, H. J.; Monti, F.; Accorsi, G.; Armaroli, N. *Angew. Chemie - Int. Ed.* **2012**, *51*, 8178–8211.

(8) Yam, V. W.-W.; Wong, K. M.-C. *Chem. Commun.* **2011**, *47*, 11579-11592.

(9) Ulbricht, C.; Beyer, B.; Friebe, C.; Winter, A.; Schubert, U. S. *Adv. Mater.* **2009**, *21*, 4418–4441.

(10) Nonoyama, M. *Bull. Chem. Soc. Jpn.* **1974**, *47*, 767–768.

(11) Sprouse, S.; King, K. A.; Spellane, P. J.; Watts, R. J. *J. Am. Chem. Soc.* **1984**, *106*, 6647–6653.

(12) Baranoff, E.; Curchod, B. F. E. *Dalton Trans.* **2015**, *44*, 8318–8329.

(13) Tamayo, A. B.; Alleyne, B. D.; Djurovich, P. I.; Lamansky, S.; Tsyba, I.; Ho, N. N.; Bau, R.; Thompson, M. E. *J. Am. Chem. Soc.* **2003**, *125*, 7377–7387.

(14) Carlson, G. A.; Djurovich, P. I.; Watts, R. J. *Inorg. Chem.* **1993**, *32*, 4483–4484.

(15) Bettington, S.; Tavasli, M.; Bryce, M. R.; Batsanov, A. S.; Thompson, A. L.; Al Attar, H. A.; Dias, F. B.; Monkman, A. P. *J. Mater. Chem.* **2006**, *16*, 1046–1052.

(16) M'hamedi, A.; Batsanov, A. S.; Fox, M. A.; Bryce, M. R.; Abdullah, K.; Al-Attar, H. A.; Monkman, A. P. *J. Mater. Chem.* **2012**, *22*, 13529–13540.

(17) Wong, M. Y.; Xie, G.; Tourbillon, C.; Sandroni, M.; Cordes, D. B.; Slawin, A. M. Z.; Samuel, I. D. W.; Zysman-Colman, E. *Dalton Trans.* **2015**, *44*, 8419–8432.

(18) Yuan, X.; Zhang, S.; Ding, Y. *Inorg. Chem. Commun.* **2012**, *17*, 26–29.

(19) Tsuboyama, A.; Takiguchi, T.; Okada, S.; Osawa, M.; Hoshino, M.; Ueno, K. *Dalton Trans.* **2004**, 1115–1116.

(20) Plummer, E. A.; Hofstraat, W.; De Cola, L. *Dalton Trans.* **2003**, 2080–2084.

(21) Auffrant, A.; Barbieri, A.; Barigelletti, F.; Lacour, J.; Mobian, P.; Collin, J.-P.; Sauvage, J.-P.; Ventura, B. *Inorg. Chem.* **2007**, *46*, 6911–6919.

(22) Whittle, V. L.; Williams, J. A. G. *Inorg. Chem.* **2008**, *47*, 6596–6607.

(23) Donato, L.; McCusker, C. E.; Castellano, F. N.; Zysman-Colman, E. *Inorg. Chem.* **2013**, *52*, 8495–8504.

(24) Xu, W.-J.; Liu, S.-J.; Zhao, X.; Zhao, N.; Liu, Z.-Q.; Xu, H.; Liang, H.; Zhao, Q.; Yu, X.-Q.; Huang, W. *Chem. Eur. J.*, **2013**, *19*, 621–629.

(25) Chandrasekhar, V.; Mahanti, B.; Bandipalli, P.; Bhanuprakash, K. *Inorg. Chem.* **2012**, *51*, 10536–10547.

(26) Andreiadis, E. S.; Imbert, D.; Pécaut, J.; Calborean, A.; Ciofini, I.; Adamo, C.; Demadrille, R.; Mazzanti, M. *Inorg. Chem.* **2011**, *50*, 8197–8206.

(27) Tennyson, A. G.; Rosen, E. L.; Collins, M. S.; Lynch, V. M.; Bielawski, C. W. *Inorg. Chem.* **2009**, *48*, 6924–6933.

(28) Lafolet, F.; Welter, S.; Popović, Z.; De Cola, L. *J. Mater. Chem.* **2005**, *15*, 2820–2828.

(29) Shin, C. H.; Huh, J. O.; Baek, S. J.; Kim, S. K.; Lee, M. H.; Do, Y. *Eur. J. Inorg. Chem.* **2010**, 3642–3651.

(30) Chi, Y.; Chou, P.-T. *Chem. Soc. Rev.* **2010**, *39*, 638–655.

(31) Choy, W. C. H.; Chan, W. K.; Yuan, Y. *Adv. Mater.* **2014**, *26*, 5368–5399.

(32) Hajra, T.; Bera, A. J. K.; Chandrasekhar, V. *Aust. J. Chem.* **2011**, *64*, 561–566.

(33) Prokhorov, A. M.; Santoro, A.; Williams, J. A. G.; Bruce, D. W. *Angew. Chem. Int. Ed. Engl.* **2012**, *51*, 95–98.

(34) Graf, M.; Czerwieniec, R.; Sünkel, K. *Zeitschrift für Anorg. und Allg. Chemie* **2013**, *639*, 1090–1094.

(35) Li, G.; Wu, Y.; Shan, G.; Che, W.; Zhu, D.; Song, B.; Yan, L.; Su, Z.; Bryce, M. R. *Chem. Commun.* **2014**, *50*, 6977–6980.

(36) Lanoë, P.-H.; Tong, C. M.; Harrington, R. W.; Probert, M. R.; Clegg, W.; Williams, J. A. G.; Kozhevnikov, V. N. *Chem. Commun.* **2014**, *50*, 6831–6834.

(37) Chandrasekhar, V.; Hajra, T.; Bera, J. K.; Rahaman, S. M. W.; Satumtira, N.; Elbjeirami, O.; Omary, M. A. *Inorg. Chem.* **2012**, *51*, 1319–1329.

(38) Daniels, R. E.; Culham, S.; Hunter, M.; Durrant, M. C.; Probert, M. R.; Clegg, W.; Williams, J. A. G.; Kozhevnikov, V. N. *Dalton Trans.* **2016**, *45*, 6949–6962.

(39) Zheng, Y.; Batsanov, A. S.; Fox, M. A.; Al-Attar, H. A.; Abdullah, K.; Jankus, V.; Bryce, M. R.; Monkman, A. P. *Angew. Chem. Int. Ed.* **2014**, *53*, 11616–11619.

(40) Yang, X.; Xu, X.; Dang, J.; Zhou, G.; Ho, C.-L.; Wong, W.-Y. *Inorg. Chem.* **2016**, *55*, 1720–1727.

(41) DeRosa, M. C.; Enright, G. D.; Evans, C. E. B.; Crutchley, R. J. *Acta Crystallogr. Sect. E.- Struct Rep.* **2005**, *61*, m967–m969.

(42) Fernández-Cestau, J.; Giménez, N.; Lalinde, E.; Montaño, P.; Moreno, M. T.; Sánchez, S. *Organometallics* **2015**, *34*, 1766–1778.

(43) Graf, M.; Sünkel, K.; Czerwieniec, R.; Böttcher, H.-C. *J. Organomet. Chem.* **2013**, *745-746*, 341–346.

(44) Hwang, F. M.; Chen, H. Y.; Chen, P. S.; Liu, C. S.; Chi, Y.; Shu, C. F.; Wu, F. I.; Chou, P. T.; Peng, S. M.; Lee, G. H. *Inorg. Chem.* **2005**, *44*, 1344–1353.

(45) Duan, J.-P.; Sun, P.-P.; Cheng, C.-H. *Adv. Mater.* **2003**, *15*, 224–228.

(46) Ono, K.; Joho, M.; Saito, K.; Tomura, M.; Matsushita, Y.; Naka, S.; Okada, H.; Onnagawa, H. *Eur. J. Inorg. Chem.* **2006**, 3676–3683.

(47) Hajra, T.; Bera, J. K.; Chandrasekhar, V. *Inorganica Chim. Acta* **2011**, *372*, 53–61.

(48) Santoro, A.; Prokhorov, A. M.; Kozhevnikov, V. N.; Whitwood, A. C.; Donnio, B.; Williams, J. A. G.; Bruce, D. W. *J. Am. Chem. Soc.* **2011**, *133*, 5248–5251.

(49) Garces, F. O.; Dedeian, K.; Keder, N. L.; Watts, R. J. *Acta Cryst. C* **1993**, *49*, 1117–1120.

(50) Bettington, S.; Thompson, A. L.; Beeby, A.; Goeta, A. E. *Acta Cryst. E* **2004**, *60*, m827–m829.

(51) McGee, K. A.; Mann, K. R. *Inorg. Chem.* **2007**, *46*, 7800–7809.

(52) Ionkin, A. S.; Wang, Y.; Marshall, W. J.; Petrov, V. A. *J. Organomet. Chem.* **2007**, *692*, 4809–4827.

(53) Norel, L.; Rudolph, M.; Vanthuyne, N.; Williams, J. A. G.; Lescop, C.; Roussel, C.; Autschbach, J.; Crassous, J.; Réau, R. *Angew. Chemie - Int. Ed.* **2010**, *49*, 99–102.

(54) Xu, C.; Wang, Z.-Q.; Dong, X.-M.; Hao, X.-Q.; Zhao, X.-M.; Ji, B.-M.; Song, M.-P. *Inorganica Chim. Acta* **2011**, *373*, 306–310.

(55) Davies, D. L.; Lowe, M. P.; Ryder, K. S.; Singh, K.; Singh, S. *Dalton Trans.* **2011**, *40*, 1028–1030.

(56) Baranoff, E.; Curchod, B. F. E.; Frey, J.; Scopelliti, R.; Kessler, F.; Tavernelli, I.; Rothlisberger, U.; Gra, M.; Nazeeruddin, K. *Inorg. Chem.* **2012**, *51*, 215–224.

(57) Baranoff, E.; Bolink, H. J.; Constable, E. C.; Delgado, M.; Häussinger, D.; Housecroft, C. E.; Nazeeruddin, M. K.; Neuburger, M.; Ortí, E.; Schneider, G. E.; Tordera, D.; Walliser, R. M.; Zampese, J. A. *Dalton Trans.* **2013**, *42*, 1073–1087.

(58) Dedeian, K.; Shi, J.; Shepherd, N.; Forsythe, E.; Morton, D. C. *Inorg. Chem.* **2005**, *44*, 4445–4447.

(59) Hanson, K.; Tamayo, A.; Diev, V. V.; Whited, M. T.; Djurovich, P. I.; Thompson, M. E. *Inorg. Chem.* **2010**, *49*, 6077–6084.

(60) Kumar, S.; Hisamatsu, Y.; Tamaki, Y.; Ishitani, O.; Aoki, S. *Inorg. Chem.* **2016**, *55*, 3829–3843.

(61) Li, P.; Shan, G. G.; Cao, H. T.; Zhu, D. X.; Su, Z. M.; Jitchati, R.; Bryce, M. R. *Eur. J. Inorg. Chem.* **2014**, 2376–2382.

(62) Constable, E. C.; Housecroft, C. E.; Kopecky, P.; Martin, C. J.; Wright, I. A; Zampese, J. A; Bolink, H. J.; Pertegas, A. *Dalton Trans.* **2013**, *42*, 8086–8103.

(63) Lamansky, S.; Djurovich, P.; Murphy, D.; Abdel-Razzaq, F.; Lee, H. E.; Adachi, C.; Burrows, P. E.; Forrest, S. R.; Thompson, M. E. *J. Am. Chem. Soc.* **2001**, *123*, 4304–4312.

(64) Zhou, X.; Burn, P. L.; Powell, B. J. *Inorg. Chem.* **2016**, *55*, 5266–5273.

(65) Sajoto, T.; Djurovich, P. I.; Tamayo, A.; Yousufuddin, M.; Bau, R.; Thompson, M. E.; Holmes, R. J.; Forrest, S. R. *Inorg. Chem.* **2005**, *44*, 7992–8003.

(66) Benjamin, H.; Zheng, Y.; Batsanov, A. S.; Fox, M. A.; Al-Attar, H. A.; Monkman, A. P.; Bryce, M. R. *Inorg. Chem.* **2016**, *55*, 8612–8627.

(67) Reineke, S.; Walzer, K.; Leo, K. *Phys. Rev. B - Condens. Matter Mater. Phys.* **2007**, *75*, 125328.

(68) Giebink, N. C.; Forrest, S. R. *Phys. Rev. B - Condens. Matter Mater. Phys.* **2008**, *77*, 235215.

(69) Tsuboyama, A.; Iwawaki, H.; Furugori, M.; Mukaide, T.; Kamatani, J.; Igawa, S.; Moriyama, T.; Miura, S.; Takiguchi, T.; Okada, S.; Hoshino, M.; Ueno, K. *J. Am. Chem. Soc.* **2003**, *125*, 12971–12979.

(70) Bolink, H. J.; De Angelis, F.; Baranoff, E.; Klein, C.; Fantacci, S.; Coronado, E.; Sessolo, M.; Kalyanasundaram, K.; Grätzel, M.; Nazeeruddin, M. K. *Chem. Commun.* **2009**, 4672–4674.

(71) Finar, I. L.; Rackham, D. M. *J. Chem. Soc. B* **1968**, 211–214.

(72) Siegrist, A. E., Patent DE1094753, 1959.

(73) Frisch, M. J.; Trucks, G.W.; Schlegel, H. B.; Scuseria, G. E.; Robb, M. A.; Cheeseman, J. R.; Scalmani, G.; Barone, V.; Mennucci, B.; Petersson, G. A.; Nakatsuji, H.; Caricato, M.; Li, X.; Hratchian, H. P.; Izmaylov, A. F.; Bloino, J.; Zheng, G.; Sonnenberg, J. L.; Hada, M.; Ehara, M.; Toyota, K.; Fukuda, R.; Hasegawa, J.; Ishida, M.; Nakajima, T.; Honda, Y.; Kitao, O.; Nakai, H.; Vreven, T.; Montgomery, Jr, J. A.; Peralta, J. E.; Ogliaro, F.; Bearpark, M.; Heyd, J. J.; Brothers, E.; Kudin, K. N.; Staroverov, V. N.; Kobayashi, R.; Normand, J.; Raghavachari, K.; Rendell, A.;

Burant, J. C.; Iyengar, S. S.; Tomasi, J.; Cossi, M.; Rega, N.; Millam, J. M.; Klene, M.; Knox, J. E.; Cross, J. B.; Bakken, V.; Adamo, C.; Jaramillo, J.; Gomperts, R.; Stratmann, R. E.; Yazyev, O.; Austin, A. J.; Cammi, R.; Pomelli, C.; Ochterski, J. W.; Martin, R. L.; Morokuma, K.; Zakrzewski, V. G.; Voth, G. A.; Salvador, P.; Dannenberg, J. J.; Dapprich, S.; Daniels, A. D.; Farkas, O.; Foresman, J. B.; Ortiz, J. V.; Cioslowski, J.; Fox, D. J. *Gaussian 09, Revision A.02*, Gaussian, Inc., Wallingford CT, 2009.

(74) Becke, A. D. *J. Chem. Phys.* **1993**, *98*, 5648-5652.

(75) Lee, C.; Yang, W.; Parr, R. G. *Phys. Rev. B* **1988**, *37*, 785–789.

(76) Hay, P. J.; Wadt, W. R. *J. Chem. Phys.* **1985**, *82*, 270–283.

(77) Wadt, W. R.; Hay, P. J. *J. Chem. Phys.* **1985**, *82*, 284–298.

(78) Hay, P. J.; Wadt, W. R. *J. Chem. Phys.* **1985**, *82*, 293–310.

(79) Petersson, G. A.; Bennett, A.; Tensfeldt, T. G.; Ailaham, M. A.; Shirley, W. A.; Mantzaris, J. *J. Chem. Phys.* **1991**, *94*, 6081–6090.

(80) Melorose, J.; Perroy, R.; Careas, S. *J. Chem. Phys.* **1988**, *89*, 2193–2218.

(81) Allouche, A.-R. *J. Comput. Chem.* **2011**, *32*, 174–182.

(82) O'Boyle, N. M.; Tenderholt, A. L.; Langner, K. M. *J. Comput. Chem.* **2008**, *29*, 839–845.

(83) Sheldrick, G.M. SADABS, version 2012/1.

(84) Sheldrick, G. M. *Acta Crystallogr.* **2008**, *A64*, 112–122.

(85) Sheldrick, G. M. *Acta Crystallogr.* **2015**, *C71*, 3–8.

(86) Bourhis, L. J.; Dolomanov, O. V; Gildea, R. J.; Howard, J. A. K.; Puschmann, H. *Acta Crystallogr.* **2015**, *A71*, 7–13.

(87) Spek, A. L. *J. Appl. Crystallogr.* **2003**, *36*, 7–13.

(88) Davidson, R.; Hsu, Y.-T.; Batchelor, T.; Yufit, D.; Beeby, A. *Dalton Trans*, **2016**, *45*, 11496-11507.

(89) Pålsson, L-O.; Monkman, A. P. *Adv. Mater.* **2002**, *14*, 757–758.

(90) Xun, S.; LeClair, G.; Zhang, J.; Chen, X.; Gao, J. P.; Wang, Z. Y. *Org. Lett.* **2006**, *8*, 1697–1700.

Insert Table of Contents artwork here